

SEEING ACROSS VIEWS: BENCHMARKING SPATIAL REASONING OF VISION-LANGUAGE MODELS IN ROBOTIC SCENES

006 **Anonymous authors**

007 Paper under double-blind review

ABSTRACT

013 Vision-language models (VLMs) are essential to Embodied AI, enabling robots
 014 to perceive, reason, and act in complex environments. They also serve as the
 015 foundation for the recent Vision-Language-Action (VLA) models. Yet most eval-
 016 uations of VLMs focus on single-view settings, leaving their ability to integrate
 017 multi-view information underexplored. At the same time, multi-camera setups
 018 are increasingly standard in robotic platforms, as they provide complementary
 019 perspectives to mitigate occlusion and depth ambiguity. Whether VLMs can ef-
 020 fectively leverage such multi-view inputs for robotic reasoning therefore remains
 021 an open question. To bridge this gap, we introduce **MV-RoboBench**, a bench-
 022 mark specifically designed to evaluate the multi-view spatial reasoning capabili-
 023 ties of VLMs in robotic manipulation. MV-RoboBench consists of 1.7k manu-
 024 ally curated QA items across eight subtasks, divided into two primary categories:
 025 spatial understanding and robotic execution. We evaluate a diverse set of exist-
 026 ing VLMs, including both open-source and closed-source models, along with en-
 027 hanced versions incorporating [Chain-of-Thought \(CoT\)](#)-inspired techniques. The
 028 results show that state-of-the-art models remain far below human performance,
 029 underscoring the substantial challenges VLMs face in multi-view robotic percep-
 030 tion. Additionally, our analysis uncovers two key findings: (i) spatial intelligence
 031 and [robotic task reasoning](#) are correlated in multi-view robotic scenarios; and (ii)
 032 strong performance on existing general-purpose single-view spatial under-
 033 standing benchmarks does not reliably translate to success in the robotic spatial tasks
 034 assessed by our benchmark. We release MV-RoboBench as an open resource to
 035 foster progress in spatially grounded VLMs and VLAs, providing a foundation for
 036 advancing embodied multi-view intelligence in robotics.

1 INTRODUCTION

040 Vision–language models (VLMs) (OpenAI, 2024; Team et al., 2023; Anthropic, 2024; Zhu
 041 et al., 2025; Bai et al., 2025; Liu et al., 2023b) play a pivotal role in Embodied AI, enabling
 042 multimodal perception and reasoning for robots while also serving as the foundation for Vi-
 043 sion–Language–Action (VLA) models (Zitkovich et al., 2023; O’Neill et al., 2024; Kim et al., 2024;
 044 Li et al., 2024; Black et al., 2024; Intelligence et al., 2025) that empower robots to operate in com-
 045 plex real-world environments. By leveraging VLMs, VLAs inherit broad multimodal competence
 046 while adding the ability to ground decisions in [physical planning and reasoning](#), positioning them
 047 as the backbone of next-generation robotic intelligence.

048 Unlike generic multimodal reasoning, robots operate in physical environments rather than abstract
 049 2D tasks. Robotic execution naturally requires *spatial intelligence*: the capacity to interpret 3D
 050 structure, reason about geometric relationships, and maintain consistency across viewpoints. Single-
 051 view inputs are inherently limited by challenges like occlusion, depth ambiguity, and restricted
 052 fields of view. *Multi-view observations*, by contrast, offer complementary perspectives that help
 053 overcome these limitations. As they become increasingly standard on robotic platforms, multi-view
 054 observations enable more robust perception and decision-making.

054
055
056
057
058
059
060 Table 1: Comparison of spatial reasoning benchmarks. Prior datasets emphasize single-view relations,
061 abstract reasoning, or non-embodied multi-view perception. **The “Partial” in “Multi-View”**
062 **indicates that these datasets contain only a subset of multi-view samples, mixed with single-view in-**
063 **puts. MV-RoboBench uniquely targets multi-view spatial reasoning within robotic manipulation**
064 **scenarios, combining embodiment with multi-view perception.**

Benchmark	Multi-View	Task Category	Environment / Scenario	Annotation	QA
EmbSpatial-Bench (Du et al., 2024)	✗	Spatial	Indoor ScanNet	Template	3.6K
Visual Spatial (Liu et al., 2023a)	✗	Spatial	MSCOCO	Template	10K
RoboSpatial (Song et al., 2025a)	✗	Spatial	Indoor tabletop	Template	3M
Spatial-MM (Shiri et al., 2024)	✗	Spatial	Internet	Template	2.3K
SpatialVLM (Chen et al., 2024)	✗	Spatial	WebLi	Template	546
VSI-Bench (Yang et al., 2025b)	✗	Spatial	Indoor egocentric video	Template	5K
OmniSpatial (Jia et al., 2025)	✗	Spatial	Internet	Manual	1.5K
ShareRobot (Eval) (Ji et al., 2025)	✗	Robotic	Robot manipulation	Manual	1.2K
ERQA (Team et al., 2025a)	Partial	Spatial + Robotic		Human-egocentric + robotic manipulation	Manual
MMSI-Bench (Yang et al., 2025c)	Partial	Spatial	Multi-Domain 3D + Egocentric + Driving		Manual
All-Angles Bench (Yeh et al., 2025)	✓	Spatial	Multi-view photos and videos	Template	2.1K
Ego3D-Bench (Gholami et al., 2025)	✓	Spatial	Egocentric 3D navigation	Template	8.6K
MV-RoboBench (Ours)	✓	Spatial + Robotic	Robot manipulation	Manual	1.7K

071
072
073 Although many benchmarks have been proposed to assess the spatial reasoning capabilities of
074 VLMs (Du et al., 2024; Liu et al., 2023a; Shiri et al., 2024; Chen et al., 2024; Song et al., 2025a; Yang
075 et al., 2025b; Jia et al., 2025), they mostly focus on single-view data. **ERQA (Team et al., 2025a)**
076 **contains only a small portion of multi-view data, and the diversity of views remains limited, and**
077 **the tasks remain relatively basic.** Moreover, they often emphasize general spatial intelligence tasks
078 while giving less attention to the embodied, action-oriented requirements of robotic manipulation.
079 ShareRobot (Ji et al., 2025) extends evaluation to embodied robotic tasks but without multi-view
080 perception. **MMSI-Bench (Yang et al., 2025c) includes multi-view tasks, but its questions primarily**
081 **target basic spatial perception and understanding.** All-Angles Bench (Yeh et al., 2025) and Ego3D-
082 Bench (Gholami et al., 2025) address multi-view reasoning, yet primarily focused on photographic
083 or navigation-related domains.

084 To fill this gap, we introduce **MV-RoboBench**, a benchmark specifically designed to evaluate multi-
085 view spatial reasoning in robotic manipulation scenarios. It is built from real robotic demonstrations
086 with synchronized multi-camera views and encompasses both spatial reasoning and robotic execu-
087 tion tasks. The benchmark includes a total of 1.7K carefully-curated QA items by humans, spanning
088 diverse manipulation tasks and environments. It offers a systematic evaluation of whether VLMs can
089 effectively integrate complementary information from multiple camera views to support decision-
090 making for robots in the real world.

091 Our key contributions are as follows:

092

- 093 • We establish the first benchmark that integrates spatial and robotic reasoning with synchro-
094 nized multi-view inputs in robotic manipulation scenarios, enabling a thorough evaluation
095 of existing open-source and closed-source VLM models.
- 096
- 097 • We show through extensive experiments that robotic multi-view scenarios remain signifi-
098 cantly challenging. The most powerful VLM models still fall far below human performance
099 and many others perform close to random. We further explore CoT-inspired enhancements,
100 which yield mixed and model-dependent effects across models.
- 101
- 102 • We provide a correlation analysis in multi-view robotic scenarios, uncovering two key find-
103 ings. First, there is a clear correlation between spatial reasoning and robotic execution.
104 Second, strong performance on general-purpose single-view spatial benchmarks, which as-
105 sess reasoning from concrete to abstract settings but are devoid of robotic context, does
106 not reliably transfer either to robotic tasks or to spatial reasoning tasks within multi-view
107 robotic scenarios. These findings highlight the unique challenges of multi-view reasoning
108 in robotics and the need for specialized benchmarks like MV-RoboBench.

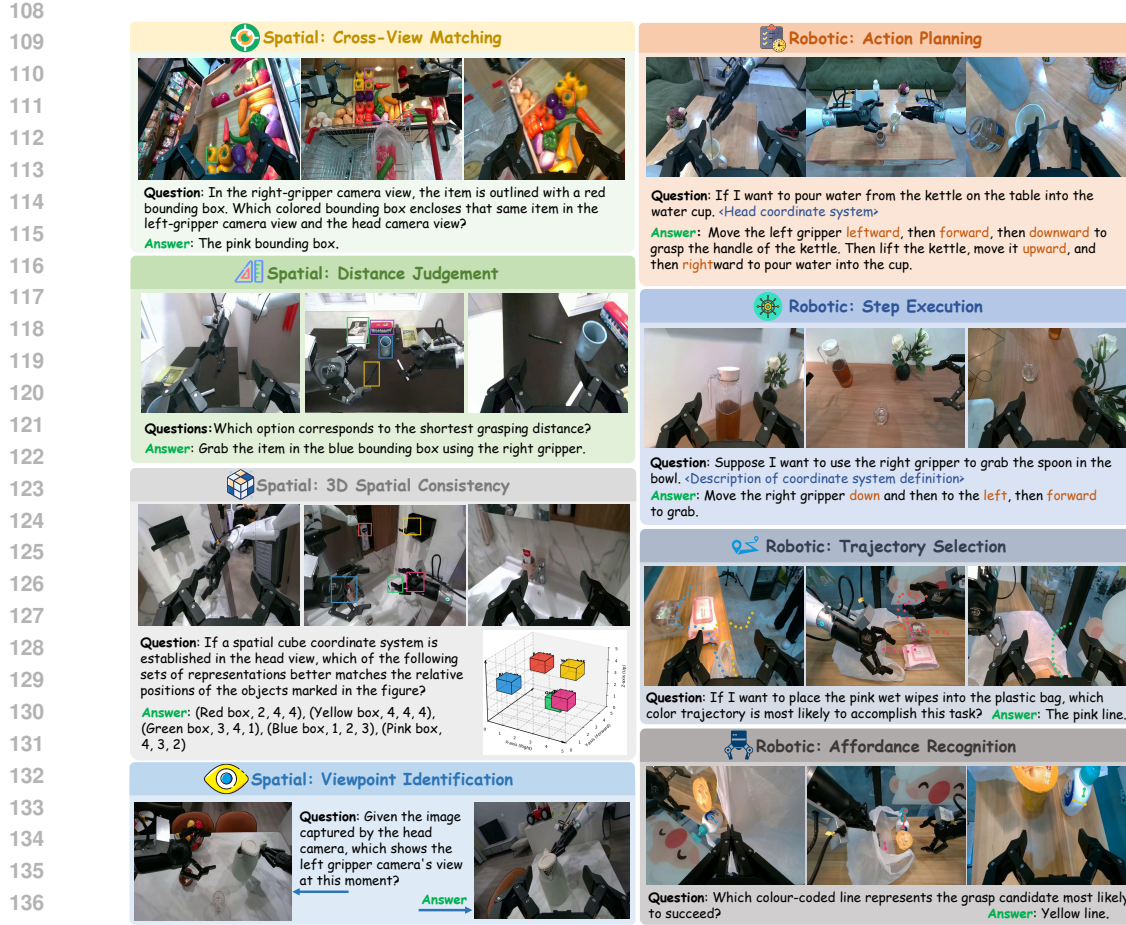


Figure 1: Representative questions from the eight tasks in **MV-RoboBench**, with *spatial* tasks shown on the left and *robotic* tasks on the right. For clarity, only simplified versions with ground-truth answers are presented here, omitting distractors. Full examples are provided in Appendix F.

2 MV-ROBOBENCH

2.1 OVERVIEW

We introduce **MV-RoboBench**, a benchmark designed to evaluate the multi-view reasoning capabilities of VLMs in robotic manipulation scenarios. It is built from the *AgiWorld* (Bu et al., 2025) and *BridgeV2* (Walke et al., 2023) datasets, spanning both single-arm and dual-arm robotic manipulation settings. In total, we construct 1,708 multiple-choice questions across eight subtasks, each with exactly one correct answer, enabling objective, reproducible, and easily extensible evaluation.

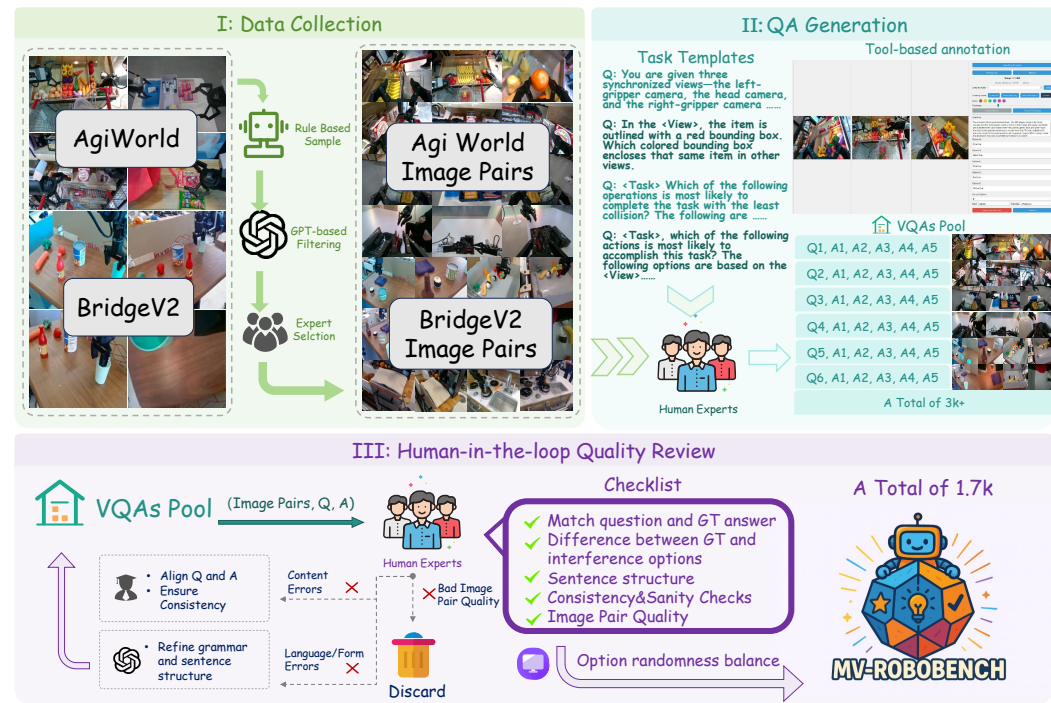
Figure 1 illustrates representative examples from the eight subtasks in MV-RoboBench. To systematically evaluate multi-view reasoning in robotic contexts, we divide the benchmark into two complementary categories: *spatial understanding* and *robotic execution*. Spatial understanding focuses on perception and reasoning across multiple camera views, assessing whether multi-view observations can be integrated into a coherent 3D representation of the scene. Robotic execution, in contrast, extends this spatial reasoning to embodied action, probing whether multi-view information can be effectively leveraged to plan, select, and validate actions in manipulation tasks.

The four *spatial understanding* subtasks each target a distinct aspect of multi-view perception: *cross-view matching* requires identifying the same object across different viewpoints; *distance judgement* evaluates relative distances between objects; *viewpoint identification* tests the ability to reason about viewpoint transformations; and *3D spatial consistency* probes whether models can maintain consis-

162 tent relative positions of objects in 3D space. Most of these subtasks rely on paired images as input,
 163 emphasizing the integration of complementary viewpoints.
 164

165 The four *robotic execution* subtasks test whether multi-view information can support robust ac-
 166 tion selection. *Action planning* requires choosing an appropriate multi-step sequence to complete
 167 a task, while *step execution* focuses on verifying whether the next single-step movement is correct.
 168 *Trajectory selection* evaluates the feasibility of candidate motion paths, and *affordance recognition*
 169 assesses the feasibility of object-specific interactions. Together, these subtasks emphasize the role of
 170 multi-view observations in resolving occlusion and depth ambiguity for embodied decision-making.
 171

172 2.2 BENCHMARK CONSTRUCTION



196 Figure 2: Construction pipeline of MV-RoboBench, consisting of three stages: data collection, QA
 197 generation, and human-in-the-loop quality review.
 198

200 We design a carefully engineered, multi-stage pipeline that has been iteratively refined to ensure the
 201 construction of high-quality QA pairs at scale (Figure 2).
 202

Data Collection. We first apply rule-based filtering to synchronized multi-view image pairs to
 203 ensure sufficient temporal separation, scene diversity, and visual clarity. GPT-4.1 then filters pairs by
 204 checking whether they satisfy at least one of the eight task definitions, after which human annotators
 205 verify clarity and appropriateness to retain only high-quality candidates for QA construction.
 206

QA Generation. For each subtask, task-specific templates were designed, and trained annotators
 207 constructed corresponding five-choice QA pairs from the curated image pairs. During annotation,
 208 we explicitly avoided designing overly ambiguous or artificially tricky questions, while ensuring
 209 that distractors remain plausible yet clearly distinguishable from the correct option. All annotated
 210 items were collected into a shared VQA pool for subsequent refinement. Further implementation
 211 details are provided in Appendices E–F.
 212

Human-in-the-loop Quality Review. Samples from the VQA pool were iteratively reviewed by
 213 trained annotators. Items that did not align with the objectives of the benchmark were discarded,
 214 while those with minor issues were revised. Content-related issues were corrected manually to
 215 maintain consistency between images and QA, while minor grammar or structural issues were re-
 fined with GPT-4.1. The revised items were then returned to the VQA pool for subsequent review
 216

AgiWorld (Unique Scenes: 597)		QAs
■ Cross-View Matching	121	
■ Distance Judgement	120	
■ Viewpoint Identification	256	
■ 3D Spatial Consistency	126	
■ Affordance Recognition	129	
■ Trajectory Selection	121	
■ Step Execution	154	
■ Action Planning	125	
Bridge (Unique Scene: 383)		Episodes
■ Cross-View Matching	80	
■ Distance Judgement	81	
■ 3D Spatial Consistency	79	
■ Affordance Recognition	81	
■ Trajectory Selection	80	
■ Step Execution	80	
■ Action Planning	80	
Total Episode	980	
Total QA	1708	

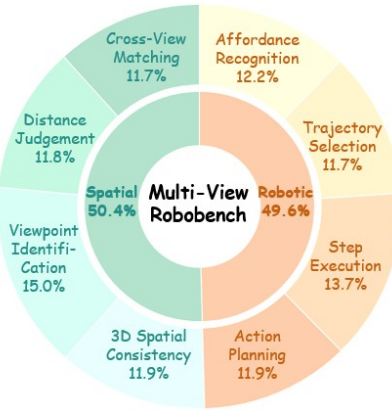


Figure 3: Data distribution of MV-RoboBench, showing QA counts per subtask and dataset source (AgiWorld and BridgeV2), and the overall balance between spatial and robotic domains.

and balancing. Accepted items were then rebalanced to randomize answer distributions, ensuring fairness and reducing bias before inclusion in the final benchmark.

Finally, Figure 3 provides a detailed breakdown of MV-RoboBench, showing both per-subtask statistics and the balance between spatial and robotic domains. In addition to the 1,708 QA pairs, the benchmark is derived from 980 episodes, highlighting its grounding in diverse real-world robotic demonstrations.

2.3 EXPLORING COT-INSPIRED ENHANCEMENTS FOR MULTI-VIEW UNDERSTANDING

Motivated by challenges unique to multi-view manipulation, including cross-view correspondence, viewpoint alignment under narrow baselines, and consistent geometric fusion, we investigate *Chain-of-Thought (CoT)*-inspired enhancements for vision–language models. Inspired by the success of CoT prompting in language reasoning, we explore three analogous directions. First, enriching visual inputs with additional scene descriptions serves as a textual CoT, explicitly verbalizing spatial context that may otherwise remain implicit; to implement this, we adopt GPT-4.1 for generating descriptions. Second, generating new perspectives through view synthesis or geometry pipelines provides a visual CoT, creating intermediate views that guide cross-perspective alignment; to implement this, we adopt VGGT (Wang et al., 2025a)¹ as a representative synthesis baseline. Third, introducing depth priors supplies a structural CoT, adding geometric constraints that reduce ambiguity in 3D reasoning; to implement this, we adopt MoGe-2 (Wang et al., 2025b) for depth estimation. Further implementation details are provided in Appendix C.

2.4 FROM PERCEPTION TO ACTION: CORRELATION ANALYSIS

The design of MV-RoboBench explicitly separates tasks into *spatial* and *robotic* categories, with the central aim of probing their correlation in multi-view manipulation scenarios. Stronger spatial reasoning is expected to support more reliable robotic execution, motivating an analysis of how perception relates to action. Beyond this internal connection, we also investigate how spatial intelligence in multi-view robotic settings compares with that measured in single-view settings. Unlike single-view tasks, which assess perception from a fixed perspective, multi-camera setups demand integrating complementary viewpoints into a coherent spatial understanding. This distinction raises two key questions: (i) how spatial and robotic reasoning relate within multi-view manipulation, and (ii) whether spatial intelligence measured in single-view settings can transfer to embodied multi-view tasks. We next provide systematic evidence on these issues in Section 4.

270 Table 2: Evaluation on **MV-RoboBench** in a zero-shot setting with a unified prompt across all mod-
 271 els. Dark purple indicates the best result and light purple the second-best within each column.
 272 Qwen2.5-vl-72B achieves the strongest performance among open-source models. GPT-5 leads the
 273 proprietary reasoning models, yet both remain far below human accuracy.
 274

275	276	277	Method	Avg.	Rank	Cross-View Match			Distance Judge	Viewpoint ID	3D Spatial Consist.	Action Plan.	Step Exec.	Trajectory Sel.	Affordance Rec.
						Spatial Tasks			Robotic Tasks						
Blind Evaluation															
279	Random Choice	19.71	–	17.80	19.40	20.00	19.07	19.41	21.54	20.65	19.81				
280	GPT-3.5-turbo	18.52	–	15.50	22.39	20.31	12.25	21.57	18.38	23.00	16.75				
	GPT-4-turbo	22.91	–	19.00	13.43	19.92	7.84	41.67	31.20	20.00	27.27				
Proprietary Models															
282	GPT-4o-mini	22.52	8	24.00	22.89	23.44	11.76	24.51	28.21	20.50	23.44				
283	GPT-4o	27.59	3	24.50	37.31	19.92	6.37	33.33	33.76	33.00	20.10				
284	GPT-4.1-nano	20.85	9	17.50	25.37	18.75	14.71	22.55	22.22	20.00	17.22				
285	GPT-4.1-mini	23.98	7	28.50	33.83	25.00	7.84	26.47	21.79	32.00	18.18				
286	GPT-4.1	30.90	1	26.00	43.28	32.03	6.37	29.90	31.62	41.50	28.23				
287	Claude-3.5	23.71	6	17.50	27.86	20.31	8.82	34.80	20.09	33.00	27.27				
	Claude-3.7	25.47	5	18.00	35.32	20.31	6.86	36.76	29.06	34.50	22.97				
	Gemini-2.0-flash	28.94	2	28.00	32.84	21.48	7.35	32.84	29.91	52.50	20.57				
	Gemini-2.5-flash	27.23	4	26.50	37.31	27.34	6.37	34.80	30.34	42.00	19.14				
Proprietary Reasoning Models															
289	o4-mini	46.47	3	21.50	48.26	26.17	65.69	74.51	63.25	44.00	25.36				
290	GPT-5-chat	31.63	7	30.00	42.79	31.64	4.90	36.76	40.17	38.00	27.75				
291	GPT-5-nano	32.75	5	21.50	33.33	17.58	56.86	39.71	35.47	31.00	26.32				
292	GPT-5-mini	38.28	4	22.00	49.25	25.78	72.55	66.18	48.72	47.00	27.75				
293	GPT-5	56.41	1	29.00	55.22	44.14	82.35	79.41	68.38	54.50	39.23				
	Claude-3.7-think	31.67	6	24.40	35.04	36.00	52.45	21.50	37.81	21.08	23.05				
	Gemini-2.5-pro	49.52	2	39.50	56.22	38.28	49.02	65.20	50.85	65.50	31.58				
Open-Source Models															
294	Gemma-3-4b	19.79	11	21.00	22.89	21.09	11.76	17.65	16.67	25.50	22.01				
295	Gemma-3-12b	20.49	9	18.00	26.37	20.31	9.80	22.55	20.94	25.50	20.57				
296	Gemma-3-27b	20.55	8	21.50	23.88	20.31	9.31	20.10	23.08	29.00	17.22				
297	InternVL3-2b	18.93	12	16.50	15.42	20.70	20.59	17.16	20.94	21.00	19.14				
298	InternVL3-8b	20.97	6	19.00	21.39	26.17	12.75	26.47	21.37	20.50	20.10				
299	InternVL3-14b	21.47	5	19.50	22.39	24.61	10.78	23.53	23.50	24.00	23.44				
300	InternVL3-38b	22.80	3	24.50	25.87	23.44	6.86	27.94	25.21	27.50	21.05				
301	InternVL3-78b	23.25	2	19.00	28.86	23.83	11.76	29.90	29.06	26.50	21.05				
302	Qwen2.5-vl-3b	20.37	10	17.50	21.89	22.66	17.65	17.16	17.95	22.00	25.84				
	Qwen2.5-vl-7b	20.84	7	20.50	20.40	20.70	8.82	22.55	26.07	24.50	22.49				
	Qwen2.5-vl-32b	22.48	4	20.50	25.87	25.39	10.78	24.51	19.66	30.50	22.49				
	Qwen2.5-vl-72b	24.29	1	20.50	34.83	27.34	4.90	28.43	27.35	29.00	24.88				
Open-Source MoE Models															
304	Llama-4-Scout	22.12	2	20.50	22.39	23.83	7.35	25.49	28.21	23.00	18.18				
305	Llama-4-Maverick	26.11	1	14.00	42.79	17.58	5.88	37.75	37.18	36.00	20.10				
Human Evaluation															
306	Human	91.04	–	95.02	94.03	92.19	93.66	86.34	89.74	87.56	89.05				

3 EVALUATION ON MV-ROBOBENCH

3.1 EVALUATION SETUP

313 We evaluate a broad spectrum of systems spanning five categories: **Blind Evaluation**, text-only
 314 LLMs without visual grounding (Random, GPT-3.5-turbo (Roumeliotis & Tsakalos, 2023), GPT-
 315 4-turbo (Achiam et al., 2023)); **Proprietary Models**, multimodal systems from major providers,
 316 including the GPT-4o family (Hurst et al., 2024), the GPT-4.1 series (OpenAI, 2024), Claude-
 317 3.5/3.7 (Anthropic, 2024), and the Gemini-2.x flash family (Team et al., 2023); **Proprietary Rea-
 318 soning Models**, architectures optimized for multi-step reasoning such as o4-mini (OpenAI, 2025b),
 319 the GPT-5 family (chat/mini/nano/full) (OpenAI, 2025a), Claude-3.7-think (Anthropic, 2024), and
 320 Gemini-2.5-pro (Team et al., 2023); **Open-Source Models**, community-developed VLMs including
 321 the Gemma-3 family (4B–27B) (Team et al., 2025b), the InternVL3 series (2B–78B) (Zhu et al.,
 322 2025), and the Qwen2.5-vl series (3B–72B) (Bai et al., 2025); and **Open-Source MoE Models**,

323 ¹We also tested several recent novel view-synthesis methods, but they performed poorly in robotic multi-
 324 view settings, especially under narrow baselines, cluttered tabletops, and gripper-centric viewpoints.

namely Llama-4-Scout and Llama-4-Maverick (Meta AI, 2025). Because all tasks are framed as multiple-choice questions, the evaluation metric is accuracy. Human evaluations were conducted separately with participants holding a computer science background to serve as a reference point. Further implementation details are provided in Appendix B.

3.2 MAIN RESULTS ON MV-ROBOBENCH

Table 2 reveals a clear progression from perception to reasoning. **Proprietary models** provide relatively stronger perception-oriented baselines, with GPT-4.1 reaching 30.90%, while **open-source VLMs** such as Qwen2.5-vl-72B (24.29%) and MoE variants like Llama-4-Maverick (26.11%) remain lower. The real improvements come from **Proprietary Reasoning Models**, where GPT-5 achieves 56.41%, with Gemini-2.5-pro (49.52%) and o4-mini (46.47%) also performing strongly. Figure 4 further contrasts the best model in each group with human performance, illustrating persistent disparities across both spatial and robotic subtasks.

Task-level analysis highlights the gap between perception and reasoning: **3D Spatial Consistency** is nearly unsolved by non-reasoning models (< 12%) yet rises to 40–82% with reasoning, largely because most models struggle to connect natural-language coordinate descriptions to 3D spatial relations. Robotic subtasks such as **Action Planning**, **Step Execution**, and **Trajectory Selection** also show substantial gains; in particular, planning benefits from the fact that more informative details are available in multi-step options compared to single-step execution. **Human evaluation** nearly solves the benchmark, reaching 91.00%, underscoring both the progress enabled by reasoning and the large remaining gap toward human-level multi-view robotic intelligence. **Furthermore, we validate the necessity of multi-view inputs in Appendix G, showing that single-view baselines suffer significant performance drops (e.g., ~19% drop in Distance Judgement for GPT-5) due to unresolved depth ambiguities.**

3.3 EVALUATION OF COT-INSPIRED ENHANCEMENTS

As shown in Table 3, the impact of CoT-inspired enhancements varies by model. For Qwen2.5-vl-7B, most add-ons bring negligible or even negative changes, with only depth showing a slight gain. Gemma-3-12B benefits substantially from CoT, while textual and synthetic views generally degrade performance. GPT-4.1, in contrast, gains most from depth priors, with textual augmentation offering smaller improvements and CoT nearly neutral. Overall, synthetic views tend to degrade performance, depth priors help only when the backbone can exploit them, and CoT is mainly useful for mid-capacity open-source models. These mixed outcomes underscore the fundamental challenge of multi-view robotic manipulation, suggesting that simple add-ons are insufficient and that progress will require tighter integration of reasoning and geometric understanding in future VLMs. Detailed implementation settings of the three enhancements are provided in Appendix C.

4 FROM PERCEPTION TO ACTION: CORRELATION AND TRANSFER

4.1 INTERNAL CORRELATION: SPATIAL VS. ROBOTIC INTELLIGENCE

As shown in Figure 5, we find evidence of a positive correlation between spatial and robotic performance in multi-view manipulation, though the strength of this relationship varies across model families. Proprietary and reasoning-oriented models exhibit a consistent trend: higher spatial accuracy tends to coincide with better **robotic planning capabilities**. In contrast, most open-source models cluster near random choice, showing limited transfer from perception to action. Overall, these findings indicate that spatial and robotic reasoning can align in sufficiently capable models, whereas the link remains tenuous in less advanced ones.

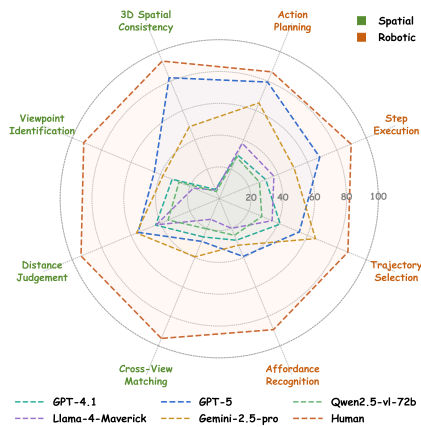
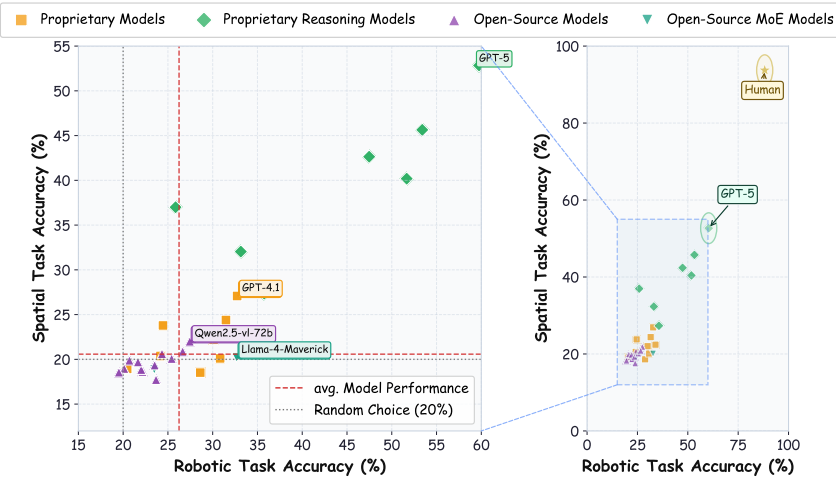


Figure 4: Best-per-group model performance across MV-RoboBench subtasks.

378 Table 3: Evaluation of *CoT-inspired enhancements* on **MV-RoboBench**. The table reports accuracy
 379 for spatial and robotic subtasks, with changes relative to the origin baseline. We evaluate four
 380 variants: **w cot** = textual CoT, **w text** = descriptive CoT, **w vgg** = visual CoT, and **w depth** =
 381 structural CoT. Color highlights mark **relative improvements** and **degradations**

Method	Avg.	Cross-View Match			Distance Judge		Viewpoint ID		3D Spatial Consist.		Δ_s	Action Plan.		Step Exec.		Trajectory Sel.		Affordance Rec.		Δ_r
		Spatial Tasks			Robotic Tasks															
Qwen2.5-vl-7b																				
origin	20.84	20.50	20.40	20.70	8.82	0.00	22.55	26.07	24.50	22.49	0.00									
w cot	20.49 (-0.35)	20.00	21.39	22.27	8.82	+0.58	22.55	23.08	25.50	22.55	-1.30									
w text	20.90 (+0.06)	20.00	20.40	22.27	4.41	-0.70	25.98	28.21	24.50	20.10	+0.82									
w vgg	20.02 (-0.82)	16.50	17.91	23.83	5.39	-1.40	21.08	25.64	23.50	24.40	-0.24									
w depth	21.14 (+0.30)	22.89	22.89	21.09	12.75	+1.04	19.12	27.35	23.50	23.44	-0.48									
Gemma-3-12B																				
origin	20.49	18.00	26.37	20.31	9.80	0.00	22.55	20.94	25.50	20.57	0.00									
w cot	24.19 (+3.70)	18.00	22.89	17.97	11.27	+0.93	21.57	27.35	27.50	25.84	+2.96									
w text	18.43 (-2.06)	19.00	21.89	21.09	7.84	-0.94	20.10	21.79	18.50	20.10	-0.47									
w vgg	18.31 (-2.18)	17.50	18.41	21.48	8.33	-1.47	18.14	22.22	19.00	24.40	+0.11									
w depth	20.41 (-0.08)	18.00	26.37	21.09	7.84	-0.18	19.12	23.50	21.00	23.44	+0.19									
GPT-4.1																				
origin	29.87	26.00	43.28	32.03	6.37	0.00	29.90	31.62	41.50	28.23	0.00									
w cot	29.84 (-0.03)	28.50	40.30	29.69	6.37	-1.21	28.92	30.34	46.00	22.49	-0.25									
w text	31.66 (+1.79)	28.00	46.50	34.38	6.86	+1.73	32.02	32.48	45.50	28.99	+1.81									
w vgg	28.02 (-1.85)	29.80	38.69	31.50	4.50	-1.54	29.21	31.17	40.50	27.45	-1.58									
w depth	33.12 (+3.25)	30.50	45.00	34.20	10.00	+3.15	31.40	33.80	47.10	28.90	+2.71									

Figure 5: Comparison of spatial and robotic task accuracy across models on **MV-RoboBench**.

4.2 EXTERNAL TRANSFERABILITY: SINGLE-VIEW TO MULTI-VIEW

To assess whether spatial intelligence measured in single-view benchmarks carries over to multi-view robotic manipulation, we use OmniSpatial (Jia et al., 2025) as a reference due to its comprehensive coverage of spatial reasoning. Our reproduced OmniSpatial results are reported in Appendix D.

Figure 6 shows that, except for *Proprietary Reasoning Models*, strong performance on single-view spatial benchmarks does not reliably transfer to MV-RoboBench, where results often remain close to random. Even among proprietary reasoning models, correlations are modest and multi-view performance lags behind single-view results. This highlights that spatial intelligence acquired in single-view settings does not seamlessly extend to the demands of multi-view robotic manipulation.

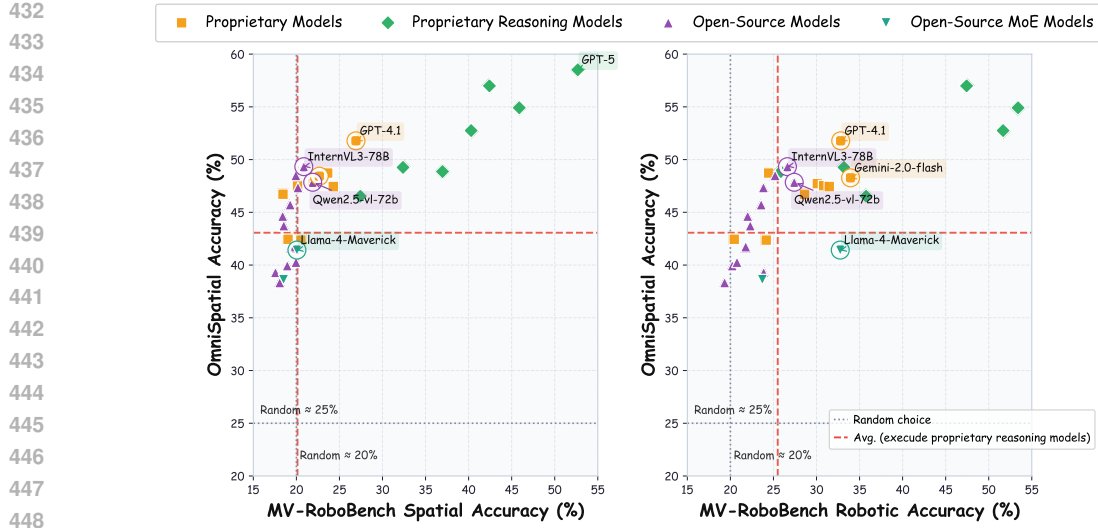


Figure 6: Comparison of model accuracies on OmniSpatial versus MV-RoboBench, with the left plot for spatial subtasks and the right plot for robotic subtasks.

5 RALATED WORKS

5.1 SPATIAL UNDERSTANDING AND REASONING IN MULTIMODAL LLM

Recent Multimodal Large Language Models (MLLMs) (OpenAI, 2025a; Hurst et al., 2024; OpenAI, 2024; Anthropic, 2024; Team et al., 2023; 2025b; Zhu et al., 2025; Bai et al., 2025; Meta AI, 2025) have demonstrated remarkable progress across diverse tasks, including captioning (Lin et al., 2024; An et al., 2024; Luo et al., 2024), retrieval (An et al., 2025), planning (Zhou et al., 2024), and even robotic tasks Zitkovich et al. (2023); O’Neill et al. (2024); Kim et al. (2024); Li et al. (2024); Black et al. (2024); Intelligence et al. (2025). Despite these advances, their ability in spatial reasoning and 3D perception remains limited, particularly when it comes to accurately interpreting depth, understanding object relationships, and reasoning about multiple perspectives or spatial configurations (Fu et al., 2024b; Song et al., 2025b; Yang et al., 2025a; Cheng et al., 2024).

To address these challenges, several specialized approaches (Cheng et al., 2024; Ma et al., 2025; Zhou et al., 2025; Fan et al., 2025; Liu et al., 2025; Cai et al., 2025; Fu et al., 2024a; Hong et al., 2023; Chen et al., 2024) have been proposed to incorporate 3D information into MLLM. Yet, such integration may disturb the pre-trained alignment between vision and language. Moreover, these models exhibit limited instruction-following ability, rarely leveraging depth information effectively when answering complex spatial reasoning (Zha et al., 2025; Li et al., 2025).

5.2 BENCHMARKING SPATIAL AND MULTI-VIEW UNDERSTANDING

Several benchmarks have been proposed to evaluate the spatial understanding capabilities of VLMs, as summarized in Table 1. Early efforts such as EmbSpatial-Bench Du et al. (2024), Visual Spatial Liu et al. (2023a), and RoboSpatial Song et al. (2025a) primarily relied on template-based question answering to assess object relationships in static scenes. Later benchmarks, including Spatial-MM Shiri et al. (2024), VSI-Bench Yang et al. (2025b), and SpatialVLM Chen et al. (2024), expanded the scope to video and egocentric settings, but their evaluations remained inherently single-view.

More recent benchmarks, such as All-Angles Bench Yeh et al. (2025) and Ego3D-Bench Gholami et al. (2025), explicitly incorporated multi-view evaluation, while OmniSpatial Jia et al. (2025) further broadened the assessment to more complex reasoning dimensions. However, these efforts primarily target general spatial understanding and fall short of addressing the embodiment and precision requirements critical for robotic manipulation. In contrast, our **MV-RoboBench** is the first

486
487
488
489
490
491
492
493
494
495
496
497
498
499
500
501
502
503
504
505
506
507
508
509
510
511
512
513
514
515
516
517
518
519
520
521
522
523
524
525
526
527
528
529
530
531
532
533
534
535
536
537
538
539
benchmark to couple multi-view spatial reasoning with robotic execution tasks, providing a realistic and comprehensive testbed for robotics.

6 DISCUSSION AND FUTURE WORK

Our study highlights three main takeaways. Our first finding is that multi-view robotic reasoning requires more than perception: perception-oriented VLMs achieve only modest improvements, and only reasoning-augmented systems approach human-level robustness. Another important observation is that spatial and robotic intelligence are closely related in multi-view manipulation, yet both remain far below human performance, underscoring the absence of robust embodied 3D reasoning. Finally, we find that competitive performance on single-view spatial benchmarks does not transfer reliably, revealing a persistent gap between reasoning in single-view settings and reasoning in multi-view robotic contexts.

Looking forward, progress will likely depend on (i) architectures that explicitly encode geometric priors and enforce multi-view consistency, (ii) training pipelines that align perception with embodied action, and (iii) larger-scale multi-camera datasets that capture the complexity of real-world manipulation. We hope MV-RoboBench can serve as both a yardstick and a catalyst for developing the next generation of spatially grounded VLMs and VLAs.

ETHICS STATEMENT

This work follows the ICLR Code of Ethics. MV-RoboBench is built entirely from publicly available robotic datasets (AgiWorld and BridgeV2) and does not involve any personally identifiable or sensitive information. All annotations were created by trained annotators under controlled conditions, and we release the benchmark for research purposes only.

REPRODUCIBILITY STATEMENT

We provide detailed descriptions of dataset construction, evaluation setup, and experimental configurations in the main text and appendix. All curated data, task templates, and evaluation code will be released in the supplementary material upon acceptance to ensure reproducibility, while maintaining anonymity during the review process.

REFERENCES

Josh Achiam, Steven Adler, Sandhini Agarwal, Lama Ahmad, Ilge Akkaya, Florencia Leoni Aleman, Diogo Almeida, Janko Altenschmidt, Sam Altman, Shyamal Anadkat, et al. Gpt-4 technical report. *arXiv preprint arXiv:2303.08774*, 2023.

Ruichuan An, Sihan Yang, Ming Lu, Renrui Zhang, Kai Zeng, Yulin Luo, Jiajun Cao, Hao Liang, Ying Chen, Qi She, et al. Mc-l lava: Multi-concept personalized vision-language model. *arXiv preprint arXiv:2411.11706*, 2024.

Ruichuan An, Sihan Yang, Renrui Zhang, Zijun Shen, Ming Lu, Gaole Dai, Hao Liang, Ziyu Guo, Shilin Yan, Yulin Luo, et al. Unictokens: Boosting personalized understanding and generation via unified concept tokens. *arXiv preprint arXiv:2505.14671*, 2025.

Anthropic. Claude 3 model card. Technical Report Version 1.0, Anthropic, 2024. URL https://www-cdn.anthropic.com/de8ba9b01c9ab7cbabf5c33b80b7bbc618857627/Model_Card_Claude_3.pdf. Accessed: 2025-09-16.

Shuai Bai, Keqin Chen, Xuejing Liu, Jialin Wang, Wenbin Ge, Sibo Song, Kai Dang, Peng Wang, Shijie Wang, Jun Tang, et al. Qwen2. 5-vl technical report. *arXiv preprint arXiv:2502.13923*, 2025.

Kevin Black, Noah Brown, Danny Driess, Adnan Esmail, Michael Equi, Chelsea Finn, Niccolo Fusai, Lachy Groom, Karol Hausman, Brian Ichter, et al. π_0 : A vision-language-action flow model for general robot control. *arXiv preprint arXiv:2410.24164*, 2024.

540 Qingwen Bu, Jisong Cai, Li Chen, Xiuqi Cui, Yan Ding, Siyuan Feng, Shenyuan Gao, Xindong
 541 He, Xuan Hu, Xu Huang, et al. Agibot world colosseo: A large-scale manipulation platform for
 542 scalable and intelligent embodied systems. *arXiv preprint arXiv:2503.06669*, 2025.

543 Wenxiao Cai, Iaroslav Ponomarenko, Jianhao Yuan, Xiaoqi Li, Wankou Yang, Hao Dong, and
 544 Bo Zhao. Spatialbot: Precise spatial understanding with vision language models. In *2025 IEEE*
 545 *International Conference on Robotics and Automation (ICRA)*, pp. 9490–9498. IEEE, 2025.

546 Boyuan Chen, Zhuo Xu, Sean Kirmani, Brain Ichter, Dorsa Sadigh, Leonidas Guibas, and Fei Xia.
 547 Spatialvilm: Endowing vision-language models with spatial reasoning capabilities. In *Proceedings*
 548 *of the IEEE/CVF Conference on Computer Vision and Pattern Recognition*, pp. 14455–14465,
 549 2024.

550 An-Chieh Cheng, Hongxu Yin, Yang Fu, Qiushan Guo, Ruihan Yang, Jan Kautz, Xiaolong Wang,
 551 and Sifei Liu. Spatialrgpt: Grounded spatial reasoning in vision-language models. *Advances in*
 552 *Neural Information Processing Systems*, 37:135062–135093, 2024.

553 Mengfei Du, Binhao Wu, Zejun Li, Xuanjing Huang, and Zhongyu Wei. Embsspatial-bench: Bench-
 554 marking spatial understanding for embodied tasks with large vision-language models. *arXiv*
 555 *preprint arXiv:2406.05756*, 2024.

556 Zhiwen Fan, Jian Zhang, Renjie Li, Junge Zhang, Runjin Chen, Hezhen Hu, Kevin Wang, Huaizhi
 557 Qu, Dilin Wang, Zhicheng Yan, et al. Vlm-3r: Vision-language models augmented with
 558 instruction-aligned 3d reconstruction. *arXiv preprint arXiv:2505.20279*, 2025.

559 Rao Fu, Jingyu Liu, Xilun Chen, Yixin Nie, and Wenhan Xiong. Scene-llm: Extending language
 560 model for 3d visual understanding and reasoning. *arXiv preprint arXiv:2403.11401*, 2024a.

561 Xingyu Fu, Yushi Hu, Bangzheng Li, Yu Feng, Haoyu Wang, Xudong Lin, Dan Roth, Noah A
 562 Smith, Wei-Chiu Ma, and Ranjay Krishna. Blink: Multimodal large language models can see but
 563 not perceive. In *European Conference on Computer Vision*, pp. 148–166. Springer, 2024b.

564 Mohsen Gholami, Ahmad Rezaei, Zhou Weimin, Yong Zhang, and Mohammad Akbari. Spa-
 565 tial reasoning with vision-language models in ego-centric multi-view scenes. *arXiv preprint*
 566 *arXiv:2509.06266*, 2025.

567 Yining Hong, Haoyu Zhen, Peihao Chen, Shuhong Zheng, Yilun Du, Zhenfang Chen, and Chuang
 568 Gan. 3d-llm: Injecting the 3d world into large language models. *Advances in Neural Information*
 569 *Processing Systems*, 36:20482–20494, 2023.

570 Aaron Hurst, Adam Lerer, Adam P Goucher, Adam Perelman, Aditya Ramesh, Aidan Clark, AJ Os-
 571 trow, Akila Welihinda, Alan Hayes, Alec Radford, et al. Gpt-4o system card. *arXiv preprint*
 572 *arXiv:2410.21276*, 2024.

573 Physical Intelligence, Kevin Black, Noah Brown, James Darpinian, Karan Dhabalia, Danny Driess,
 574 Adnan Esmail, Michael Equi, Chelsea Finn, Niccolo Fusai, et al. $\pi\{0.5\}$: a vision-language-
 575 action model with open-world generalization. *arXiv preprint arXiv:2504.16054*, 2025.

576 Yuheng Ji, Huajie Tan, Jiayu Shi, Xiaoshuai Hao, Yuan Zhang, Hengyuan Zhang, Pengwei Wang,
 577 Mengdi Zhao, Yao Mu, Pengju An, et al. Robobrain: A unified brain model for robotic manipu-
 578 lation from abstract to concrete. In *Proceedings of the Computer Vision and Pattern Recognition*
 579 *Conference*, pp. 1724–1734, 2025.

580 Mengdi Jia, Zekun Qi, Shaochen Zhang, Wenyao Zhang, Xinqiang Yu, Jiawei He, He Wang, and
 581 Li Yi. Omnispatial: Towards comprehensive spatial reasoning benchmark for vision language
 582 models. *arXiv preprint arXiv:2506.03135*, 2025.

583 Haian Jin, Hanwen Jiang, Hao Tan, Kai Zhang, Sai Bi, Tianyuan Zhang, Fujun Luan, Noah Snavely,
 584 and Zexiang Xu. Lvsm: A large view synthesis model with minimal 3d inductive bias. *arXiv*
 585 *preprint arXiv:2410.17242*, 2024.

586 Moo Jin Kim, Karl Pertsch, Siddharth Karamcheti, Ted Xiao, Ashwin Balakrishna, Suraj Nair,
 587 Rafael Rafailov, Ethan Foster, Grace Lam, Pannag Sanketi, et al. Openvla: An open-source
 588 vision-language-action model. *arXiv preprint arXiv:2406.09246*, 2024.

594 Haoyuan Li, Yanpeng Zhou, Yufei Gao, Tao Tang, Jianhua Han, Yujie Yuan, Dave Zhenyu Chen,
 595 Jiawang Bian, Hang Xu, and Xiaodan Liang. Does your 3d encoder really work? when pretrain-
 596 sft from 2d vlms meets 3d vlms. *arXiv preprint arXiv:2506.05318*, 2025.

597

598 Qixiu Li, Yaobo Liang, Zeyu Wang, Lin Luo, Xi Chen, Mozheng Liao, Fangyun Wei, Yu Deng,
 599 Sicheng Xu, Yizhong Zhang, et al. Cogact: A foundational vision-language-action model for
 600 synergizing cognition and action in robotic manipulation. *arXiv preprint arXiv:2411.19650*, 2024.

601 Weifeng Lin, Xinyu Wei, Ruichuan An, Peng Gao, Bocheng Zou, Yulin Luo, Siyuan Huang, Shang-
 602 hang Zhang, and Hongsheng Li. Draw-and-understand: Leveraging visual prompts to enable
 603 mllms to comprehend what you want. *arXiv preprint arXiv:2403.20271*, 2024.

604

605 Fangyu Liu, Guy Emerson, and Nigel Collier. Visual spatial reasoning. *Transactions of the Associa-
 606 tion for Computational Linguistics*, 11:635–651, 2023a.

607

608 Haotian Liu, Chunyuan Li, Qingyang Wu, and Yong Jae Lee. Visual instruction tuning. *Advances
 609 in neural information processing systems*, 36:34892–34916, 2023b.

610

611 Yang Liu, Ming Ma, Xiaomin Yu, Pengxiang Ding, Han Zhao, Mingyang Sun, Siteng Huang, and
 612 Donglin Wang. Ssr: Enhancing depth perception in vision-language models via rationale-guided
 613 spatial reasoning. *arXiv preprint arXiv:2505.12448*, 2025.

614

615 Yulin Luo, Ruichuan An, Bocheng Zou, Yiming Tang, Jiaming Liu, and Shanghang Zhang. Llm
 616 as dataset analyst: Subpopulation structure discovery with large language model. In *European
 617 Conference on Computer Vision*, pp. 235–252. Springer, 2024.

618

619 Wufei Ma, Luoxin Ye, Celso M de Melo, Alan Yuille, and Jieneng Chen. Spatialllm: A compound
 620 3d-informed design towards spatially-intelligent large multimodal models. In *Proceedings of the
 621 Computer Vision and Pattern Recognition Conference*, pp. 17249–17260, 2025.

622

623 Meta AI. The llama 4 herd: The beginning of a new era of natively multimodal ai in-
 624 novation. <https://ai.meta.com/blog/llama-4-multimodal-intelligence/>,
 625 April 5 2025. Accessed: 2025-09-16.

626

627 OpenAI. Gpt-4.1. <https://openai.com/index/gpt-4-1/>, 2024. Accessed: 2025-09-12.

628

629 OpenAI. Gpt-5 technical report. <https://cdn.openai.com/gpt-5-system-card.pdf>,
 630 2025a. Accessed September 24, 2025.

631

632 OpenAI. Openai o3 and o4-mini system card. <https://openai.com/research/o3-o4-mini-system-card>, 2025b. Accessed September 24, 2025.

633

634 Abby O’Neill, Abdul Rehman, Abhiram Maddukuri, Abhishek Gupta, Abhishek Padalkar, Abraham
 635 Lee, Acorn Pooley, Agrim Gupta, Ajay Mandlekar, Ajinkya Jain, et al. Open x-embodiment:
 636 Robotic learning datasets and rt-x models: Open x-embodiment collaboration 0. In *2024 IEEE
 637 International Conference on Robotics and Automation (ICRA)*, pp. 6892–6903. IEEE, 2024.

638

639 Luigi Piccinelli, Christos Sakaridis, Yung-Hsu Yang, Mattia Segu, Siyuan Li, Wim Abbeloos, and
 640 Luc Van Gool. Unidepthv2: Universal monocular metric depth estimation made simpler. *arXiv
 641 preprint arXiv:2502.20110*, 2025.

642

643 Konstantinos I Roumeliotis and Nikolaos D Tsakiris. Chatgpt and open-ai models: A preliminary
 644 review. *Future Internet*, 15(6):192, 2023.

645

646 Fatemeh Shiri, Xiao-Yu Guo, Mona Golestan Far, Xin Yu, Gholamreza Haffari, and Yuan-Fang Li.
 647 An empirical analysis on spatial reasoning capabilities of large multimodal models. *arXiv preprint
 648 arXiv:2411.06048*, 2024.

649

650 Chan Hee Song, Valts Blukis, Jonathan Tremblay, Stephen Tyree, Yu Su, and Stan Birchfield. Ro-
 651 bospatial: Teaching spatial understanding to 2d and 3d vision-language models for robotics.
 652 In *Proceedings of the Computer Vision and Pattern Recognition Conference*, pp. 15768–15780,
 653 2025a.

648 Chan Hee Song, Valts Blukis, Jonathan Tremblay, Stephen Tyree, Yu Su, and Stan Birchfield. Ro-
 649 bospatial: Teaching spatial understanding to 2d and 3d vision-language models for robotics.
 650 In *Proceedings of the Computer Vision and Pattern Recognition Conference*, pp. 15768–15780,
 651 2025b.

652 Gemini Team, Rohan Anil, Sebastian Borgeaud, Jean-Baptiste Alayrac, Jiahui Yu, Radu Soricut,
 653 Johan Schalkwyk, Andrew M Dai, Anja Hauth, Katie Millican, et al. Gemini: a family of highly
 654 capable multimodal models. *arXiv preprint arXiv:2312.11805*, 2023.

655 Gemini Robotics Team, Saminda Abeyruwan, Joshua Ainslie, Jean-Baptiste Alayrac, Montser-
 656 rat Gonzalez Arenas, Travis Armstrong, Ashwin Balakrishna, Robert Baruch, Maria Bauza,
 657 Michiel Blokzijl, et al. Gemini robotics: Bringing ai into the physical world. *arXiv preprint*
 658 *arXiv:2503.20020*, 2025a.

659 Gemma Team, Aishwarya Kamath, Johan Ferret, Shreya Pathak, Nino Vieillard, Ramona Merhej,
 660 Sarah Perrin, Tatiana Matejovicova, Alexandre Ramé, Morgane Rivière, et al. Gemma 3 technical
 661 report. *arXiv preprint arXiv:2503.19786*, 2025b.

662 Homer Rich Walke, Kevin Black, Tony Z Zhao, Quan Vuong, Chongyi Zheng, Philippe Hansen-
 663 Estruch, Andre Wang He, Vivek Myers, Moo Jin Kim, Max Du, et al. Bridgedata v2: A dataset
 664 for robot learning at scale. In *Conference on Robot Learning*, pp. 1723–1736. PMLR, 2023.

665 Jianyuan Wang, Minghao Chen, Nikita Karaev, Andrea Vedaldi, Christian Rupprecht, and David
 666 Novotny. Vggt: Visual geometry grounded transformer. In *Proceedings of the Computer Vision*
 667 and *Pattern Recognition Conference*, pp. 5294–5306, 2025a.

668 Ruicheng Wang, Sicheng Xu, Yue Dong, Yu Deng, Jianfeng Xiang, Zelong Lv, Guangzhong Sun,
 669 Xin Tong, and Jiaolong Yang. Moge-2: Accurate monocular geometry with metric scale and
 670 sharp details. *arXiv preprint arXiv:2507.02546*, 2025b.

671 Yifan Wang, Jianjun Zhou, Haoyi Zhu, Wenzheng Chang, Yang Zhou, Zizun Li, Junyi Chen, Jiang-
 672 miao Pang, Chunhua Shen, and Tong He. π^3 : Scalable permutation-equivariant visual geometry
 673 learning. *arXiv preprint arXiv:2507.13347*, 2025c.

674 Jianfeng Xiang, Zelong Lv, Sicheng Xu, Yu Deng, Ruicheng Wang, Bowen Zhang, Dong Chen,
 675 Xin Tong, and Jiaolong Yang. Structured 3d latents for scalable and versatile 3d generation.
 676 In *Proceedings of the Computer Vision and Pattern Recognition Conference*, pp. 21469–21480,
 677 2025.

678 Jiale Xu, Weihao Cheng, Yiming Gao, Xintao Wang, Shenghua Gao, and Ying Shan. Instantmesh:
 679 Efficient 3d mesh generation from a single image with sparse-view large reconstruction models.
 680 *arXiv preprint arXiv:2404.07191*, 2024.

681 Jihan Yang, Shusheng Yang, Anjali W Gupta, Rilyn Han, Li Fei-Fei, and Saining Xie. Thinking in
 682 space: How multimodal large language models see, remember, and recall spaces. In *Proceedings*
 683 of the *Computer Vision and Pattern Recognition Conference*, pp. 10632–10643, 2025a.

684 Jihan Yang, Shusheng Yang, Anjali W Gupta, Rilyn Han, Li Fei-Fei, and Saining Xie. Thinking in
 685 space: How multimodal large language models see, remember, and recall spaces. In *Proceedings*
 686 of the *Computer Vision and Pattern Recognition Conference*, pp. 10632–10643, 2025b.

687 Sihan Yang, Runsen Xu, Yiman Xie, Sizhe Yang, Mo Li, Jingli Lin, Chenming Zhu, Xiaochen
 688 Chen, Haodong Duan, Xiangyu Yue, et al. Mmsi-bench: A benchmark for multi-image spatial
 689 intelligence. *arXiv preprint arXiv:2505.23764*, 2025c.

690 Chun-Hsiao Yeh, Chenyu Wang, Shengbang Tong, Ta-Ying Cheng, Ruoyu Wang, Tianzhe Chu,
 691 Yuexiang Zhai, Yubei Chen, Shenghua Gao, and Yi Ma. Seeing from another perspective: Eval-
 692 uating multi-view understanding in mllms. *arXiv preprint arXiv:2504.15280*, 2025.

693 Jirong Zha, Yuxuan Fan, Xiao Yang, Chen Gao, and Xinlei Chen. How to enable llm with 3d
 694 capacity? a survey of spatial reasoning in llm. *arXiv preprint arXiv:2504.05786*, 2025.

702 Enshen Zhou, Jingkun An, Cheng Chi, Yi Han, Shanyu Rong, Chi Zhang, Pengwei Wang,
703 Zhongyuan Wang, Tiejun Huang, Lu Sheng, et al. Roborefer: Towards spatial referring with
704 reasoning in vision-language models for robotics. *arXiv preprint arXiv:2506.04308*, 2025.

705 Xingcheng Zhou, Mingyu Liu, Ekim Yurtsever, Bare Luka Zagar, Walter Zimmer, Hu Cao, and
706 Alois C Knoll. Vision language models in autonomous driving: A survey and outlook. *IEEE*
707 *Transactions on Intelligent Vehicles*, 2024.

708 Jinguo Zhu, Weiyun Wang, Zhe Chen, Zhaoyang Liu, Shenglong Ye, Lixin Gu, Hao Tian, Yuchen
709 Duan, Weijie Su, Jie Shao, et al. Internvl3: Exploring advanced training and test-time recipes for
710 open-source multimodal models. *arXiv preprint arXiv:2504.10479*, 2025.

711 Brianna Zitkovich, Tianhe Yu, Sichun Xu, Peng Xu, Ted Xiao, Fei Xia, Jialin Wu, Paul Wohlhart,
712 Stefan Welker, Ayzaan Wahid, et al. Rt-2: Vision-language-action models transfer web knowledge
713 to robotic control. In *Conference on Robot Learning*, pp. 2165–2183. PMLR, 2023.

714

715

716

717

718

719

720

721

722

723

724

725

726

727

728

729

730

731

732

733

734

735

736

737

738

739

740

741

742

743

744

745

746

747

748

749

750

751

752

753

754

755

756 **A APPENDIX OVERVIEW**
757758 In these supplementary materials, we provide additional details to complement the main paper:
759

- 760 • **Appendix B:** Experimental setup details, including system prompts, inference configurations,
761 and hyperparameter settings for all evaluated models (see Appendix B).
- 762 • **Appendix C:** Implementation details of CoT-inspired enhancements, including prompts
763 used for textual augmentation, pipelines for visual augmentation, and configuration for
764 depth priors (see Appendix C).
- 765 • **Appendix D:** Complete evaluation setup and results on external benchmarks, covering both
766 *OmniSpatial* and *ERQA* experiments (see Appendix D).
- 767 • **Appendix E:** Preparations for building the benchmark, including dataset setup and annotation
768 tool design (see Appendix E).
- 769 • **Appendix F:** Detailed process of benchmark construction, including task formulation
770 methodology and annotation workflow (see Appendix F).
- 771 • **Appendix G:** Ablation study demonstrating the necessity of multi-view inputs by comparing
772 performance against single-view baselines (see Appendix G).
- 773 • **Appendix H:** Analysis of model sensitivity to image orientation (see Appendix H).
- 774 • **Appendix I:** Evaluation of model capability to determine "no correct choice" (see Ap-
775 pendix I).
- 776 • **Appendix J:** Qualitative error analysis of representative model failures on MV-RoboBench,
777 covering single-view bias, depth and occlusion confusion, frame-of-reference errors, and
778 affordance misunderstandings (see Appendix J).

781 **B EXPERIMENTAL SETUP**
782783 This appendix provides additional details of the experimental setup used in our evaluation.
784785 **B.1 MODEL ACCESS AND INFERENCE PROTOCOL**
786787 All models were evaluated in a *zero-shot* setting with a unified protocol across tasks. Proprietary
788 systems were accessed through their official APIs, while open-source models were run via Hugging-
789 Face implementations.
790791 **B.2 PROMPT TEMPLATES**
792793 For reproducibility, we report the exact system- and user-level instructions used across all experi-
794 ments.
795796 **SYSTEM PROMPT**
797798 We employed the following JSON-formatted system instruction:
799

```

800 1 {
801 2   "role": "system",
802 3   "content": "You are an AI assistant performing a harmless academic
803 4       robotics benchmark evaluation. All content is for research purposes.
804 5       You are an evaluator for a robotic vision benchmark.
805 6       You will be shown a multiple-choice question and a set of candidate
806 7       answers, sometimes with images.
807 8       Your task is to carefully read the question, consider the provided
808 9       information, and then select the SINGLE best option (A, B, C, D, or
809 E).
810 9       Guidelines:

```

```

810 10 - Always base your answer only on the question and the provided options/
811 11 images.
812 12 - Do not use external knowledge beyond what is shown.
813 12 - Output strictly one option letter (A/B/C/D/E).
814 13 - Do not explain your reasoning unless explicitly requested.
815 14 - If multiple answers seem plausible, choose the most consistent with
816 15 the given views.
817 16 Answer format:
818 17 Answer: <option letter>"
```

819 18 }

820

821

USER PROMPT

822

823 Each QA item was wrapped into the following template, where `question` denotes the natural-
 824 language question and `opts_str` is the list of candidate options. The corresponding images
 825 (base64-encoded) were attached alongside the prompt.

826

```

827 1 Question:
828 2 {question}
829 3
830 4 Options:
831 5 {opts_str}
832 6
833 7 Please output a single line of the form:
834 8 'Answer: X' where X is one of A, B, C, D, E.
```

835

B.3 IMAGE ENCODING

836

837 All images were provided in base64-encoded format. We followed the OpenAI-style API conven-
 838 tion:

```

839 1 def encode_image_to_base64(image_path: Path) -> str:
840 2     with open(image_path, "rb") as f:
841 3         return base64.b64encode(f.read()).decode("utf-8")
```

843

Encoded images were attached to the user message under the "image" field.

844

845

B.4 EVALUATION PROTOCOL

846

847 All tasks are framed as multiple-choice QA. Accuracy was computed as the fraction of correctly
 848 predicted answers. Each model was evaluated over the entire benchmark without post-hoc filtering.
 849 We ensured identical question order and random seeds across runs for fair comparison.

850

851

B.5 HUMAN EVALUATION

852

853 We recruited five participants with strong backgrounds in computer science, including PhD, mas-
 854 ter's, and senior undergraduate students, none of whom were involved in dataset annotation. All
 855 participants completed the benchmark under the same interface without access to model outputs.
 856 To ensure a fair comparison, we did not impose time limits or prohibit external references, since
 857 state-of-the-art models also leverage extensive Internet-scale data. We report the average accuracy
 858 of the participants as an approximate human upper bound.

859

860

C IMPLEMENTATION OF CoT-INSPIRED ENHANCEMENTS

861

862

863

This appendix provides implementation details for the three CoT-inspired enhancement strategies
 explored in Section

864
865

C.1 CHAIN-OF-THOUGHT (COT) PROMPTING

866

We keep the system prompt unchanged and prepend a single sentence to the *user* prompt:

867

868

1 You are a careful, step-by-step reasoner. Think concisely.

869

870

The rest of the user template (question, options, and answer format) remains identical to the zero-shot setting in Appendix B.

871

872

873

C.2 TEXTUAL AUGMENTATION

874

875

To supply richer spatial context, we generated a holistic scene description from the multi-view images using GPT-4.1 (OpenAI, 2024). We prompted the model as:

876

877

1 These images provide multiple views of the same scene.
2 Based on `all` of them, provide a single, holistic paragraph
3 describing the entire scene `and` the spatial relationship
4 between the objects.

878

879

The generated paragraph was inserted verbatim into the user prompt under a `Context` : header, immediately before the QA item.

880

881

882

883

884

885

C.3 VISUAL AUGMENTATION VIA NOVEL VIEW SYNTHESIS

886

887

To provide cross-view alignment signals, we generated synthetic intermediate views between existing camera perspectives. We experimented with several families of novel view synthesis (NVS) methods:

888

889

890

891

892

893

894

895

896

897

898

899

900

901

902

903

904

905

906

907

- **Object-centric synthesis.** Methods such as InstantMesh (Xu et al., 2024) and Trellis (Xi-ang et al., 2025) are designed for reconstructing individual objects from sparse views. While effective for clean object-level inputs, they proved unsuitable for cluttered robotic scenes, as selecting accurate masks is non-trivial and the outputs often failed to preserve global scene layout (see Appendix Figure 7).

908

909

910

911

912

913

914

915

916

917

- **Scene-level synthesis.** LVSM (Jin et al., 2024) attempts to interpolate between camera poses with minimal 3D inductive bias. In our robotic setup (e.g., gripper and head-mounted cameras), interpolated views were severely blurred and inconsistent, particularly under narrow baselines and cluttered tabletops (Appendix Figure 8).

918

919

920

921

922

923

924

925

926

927

928

929

930

931

932

933

934

935

936

937

938

939

940

941

942

943

944

945

946

947

948

In practice, we adopted VGGT to generate one interpolated frame between each camera pair, resized to 224×224 , and attached it as an additional input.

949

950

951

952

953

954

955

956

957

958

959

960

961

962

963

964

965

966

967

968

C.4 STRUCTURAL AUGMENTATION VIA DEPTH PRIORS

959

960

961

962

963

964

965

966

967

968

969

970

971

972

973

974

975

To provide models with explicit geometric constraints, we augmented each view with predicted depth maps. We considered recent monocular depth estimation approaches, including UniDepthV2 (Piccinelli et al., 2025), but ultimately adopted MoGe-2 (Wang et al., 2025b) as it proved more robust in cluttered indoor manipulation scenes.

976

977

978

979

980

981

982

983

984

985

986

987

988

989

990

991

992

993

994

995

996

997

998

999



Figure 7: Failure of object-centric synthesis (Trellis). *Top*: original inputs; *Bottom*: synthesized views that fail to capture the full scene.

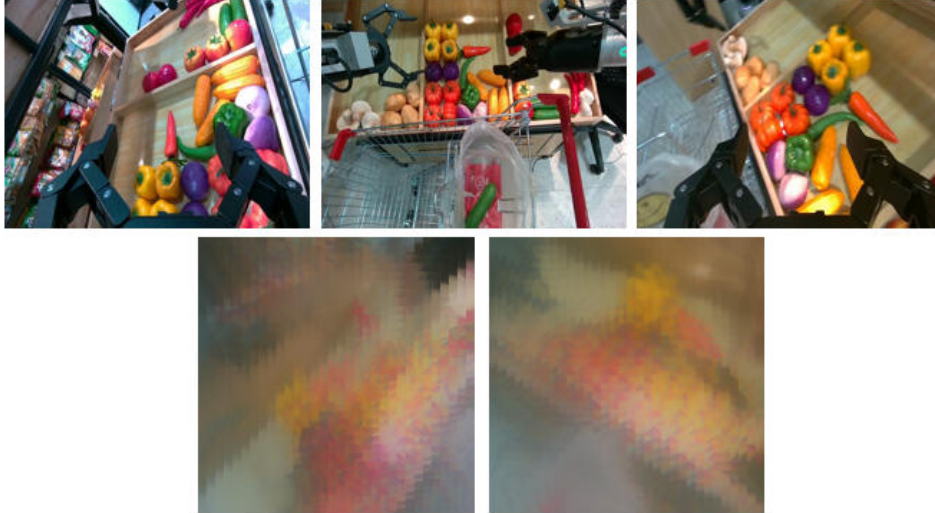


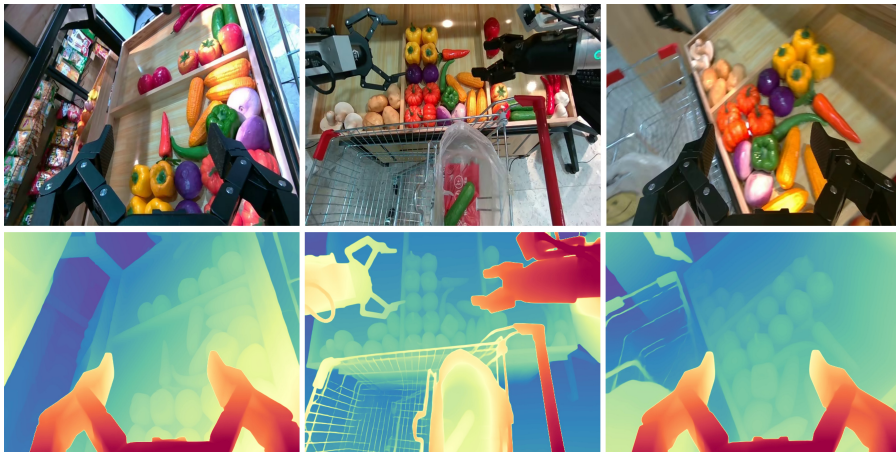
Figure 8: Failure of LVSM scene interpolation. *Top*: original inputs from left gripper, head, and right gripper cameras; *Bottom*: blurry synthesized view from interpolated extrinsics.

"text": "Image context: Corresponding estimated depth map.
In this depth map, red areas indicate objects that are closer,
and blue areas indicate objects that are farther away."

This additional channel allowed the model to incorporate depth priors when reasoning about occluded or overlapping objects, thereby reducing spatial ambiguity.

D EVALUATION ON EXTERNAL SPATIAL BENCHMARKS

Our study focuses on spatial intelligence within robotic operation scenarios. To provide a broader context, we include the **OmniSpatial** benchmark, which spans an unusually comprehensive range of spatial intelligence tasks, from abstract reasoning to concrete domain understanding. Incorporating OmniSpatial allows us to assess whether the spatial intelligence exhibited by models in general cognitive benchmarks is consistent with their performance in robotics-specific tasks. Table 4 reports

972
973
974
975
976
977
978
979
980
981
982
983984
985
986
987
Figure 9: Successful geometry-guided synthesis with VGGT. *Top*: original inputs; *Bottom*: interpolated
novel view that preserves object layout and spatial relations.988
989
990
991
992
993
994
995
996
997
998
999
1000
10011002
1003
1004
1005
1006
1007
1008
1009
1010
1011
1012
1013
1014
1015
1016
1017
1018
1019
1020
1021
1022
1023
1024
1025
Figure 10: Structural augmentation via depth priors. The top row shows the original RGB images; the bottom row shows the corresponding MoGe-2 depth predictions (red indicates closer, blue indicates farther).

these results, where asterisked entries (*) indicate our reproductions, and the remaining scores are taken directly from the OmniSpatial paper to maintain fairness and comparability.

D.1 ADDITIONAL EVALUATION ON ERQA

Following the reviewers' suggestions, we also evaluated our models on the ERQA benchmark to investigate domain-specific transferability. ERQA focuses on embodied reasoning in simulated environments and includes categories such as Action Reasoning, State Estimation, and a subset of Multi-view Reasoning.

Table 5 reports the detailed performance. While ERQA is domain-relevant, our analysis suggests that it exhibits **low discriminative power** for comparing current SOTA models:

- **Compressed Performance Range:** The overall accuracy gap between smaller open-source models (e.g., Qwen2.5-vl-7b at 43.11%) and SOTA proprietary models (e.g., GPT-4o at 46.00%) is marginally narrow (< 3%).
- **Lack of Gradient:** Most models cluster tightly between 40% and 50% across most sub-tasks. This "flat" distribution makes it difficult to observe meaningful statistical correlations between model capability and downstream robotic performance.

1026 Table 4: Comparison of model performance on **OmniSpatial**, covering four categories: dynamic
 1027 reasoning, spatial interaction, complex logic, and perspective taking. Results are reported as average
 1028 accuracy (%), with asterisked rows (*) denoting our reproduced results.

1030	1031	1032	Method	1033		1034			1035		1036			1037			1038			1039			1040			1041			1042			1043			1044			1045			1046			1047			1048			1049			1050			1051			1052			1053			1054			1055			1056			1057			1058			1059			1060			1061			1062			1063			1064			1065			1066			1067			1068			1069			1070			1071			1072			1073			1074			1075			1076			1077			1078			1079		
1033				1034			1035		1036		1037			1038			1039			1040			1041			1042			1043			1044			1045			1046			1047			1048			1049			1050			1051			1052			1053			1054			1055			1056			1057			1058			1059			1060			1061			1062			1063			1064			1065			1066			1067			1068			1069			1070			1071			1072			1073			1074			1075			1076			1077			1078			1079					
1033				1034			1035		1036		1037			1038			1039			1040			1041			1042			1043			1044			1045			1046			1047			1048			1049			1050			1051			1052			1053			1054			1055			1056			1057			1058			1059			1060			1061			1062			1063			1064			1065			1066			1067			1068			1069			1070			1071			1072			1073			1074			1075			1076			1077			1078			1079					
1033				1034			1035		1036		1037			1038			1039			1040			1041			1042			1043			1044			1045			1046			1047			1048			1049			1050			1051			1052			1053			1054			1055			1056			1057			1058			1059			1060			1061			1062			1063			1064			1065			1066			1067			1068			1069			1070			1071			1072			1073			1074			1075			1076			1077			1078			1079					
1033				1034			1035		1036		1037			1038			1039			1040			1041			1042			1043			1044			1045			1046			1047			1048			1049			1050			1051			1052			1053			1054			1055			1056			1057			1058			1059			1060			1061			1062			1063			1064			1065			1066			1067			1068			1069			1070			1071			1072			1073			1074			1075			1076			1077			1078			1079					
1033				1034			1035		1036		1037			1038			1039			1040			1041			1042			1043			1044			1045			1046			1047			1048			1049			1050			1051			1052			1053			1054			1055			1056			1057			1058			1059			1060			1061			1062			1063			1064			1065																																															

1080 Table 5: Evaluation results on the ERQA benchmark. Results are reported as accuracy (%). Note
 1081 the relatively narrow performance gap between open-source and proprietary models compared to
 1082 MV-RoboBench or OmniSpatial.

1083

1084	Method	Avg.	Action Reasoning	Multi-view Reasoning	Other	Pointing	Spatial Reasoning	State Estimation	Task Reasoning
<i>Proprietary Reasoning Models</i>									
1086	GPT-5	59.34	65.71	33.33	33.33	82.35	58.33	69.81	60.53
1087	GPT-5-mini	54.00	54.17	32.43	42.86	55.88	58.33	61.82	65.79
1088	GPT-5-chat	49.50	50.00	35.14	28.57	61.76	52.38	60.00	55.26
1089	GPT-5-nano	44.00	45.83	21.62	21.43	52.94	50.00	49.09	50.00
<i>Proprietary Models</i>									
1090	GPT-4.1	49.00	56.94	40.54	21.43	55.88	46.43	56.36	57.89
1091	GPT-4o	46.00	41.67	27.03	28.57	61.76	48.81	54.55	47.37
1092	GPT-4.1-mini	46.00	37.50	40.54	28.57	50.00	45.24	56.36	60.53
1093	GPT-4.1-nano	38.25	37.50	21.62	14.29	32.35	38.10	50.91	60.53
<i>Open-Source Models</i>									
1094	Qwen2.5-vl-72b	44.61	41.67	16.67	21.43	52.94	63.10	49.09	50.00
1095	Qwen2.5-vl-32b	44.75	38.89	32.43	21.43	58.82	52.38	54.55	47.37
1096	Qwen2.5-vl-7b	43.11	37.50	20.00	18.18	55.88	43.37	56.36	55.56

1096

1097

1098

1099

1100

1101

1102

1103

1104

1105

1106

1107

1108

1109

1110

1111

1112

1113

1114

1115

1116

1117

1118 Figure 11: Annotation interface of the AgiWorld label tool, implemented with Qt on Windows. The
 1119 design emphasizes clarity and ease of use for multi-view annotation.

1120

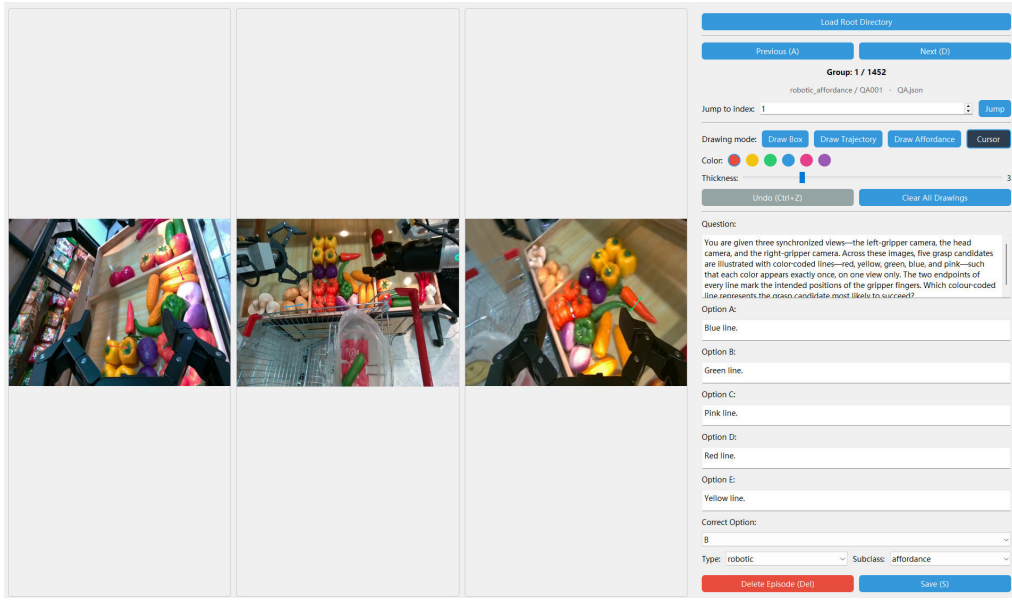
1121

1122

1123 E.2 PRE-GENERATION OF IMAGE PAIRS

1125 Before QA construction, we first pre-generated candidate image pairs from both datasets. For the
 1126 AgiWorld dataset, we randomly sampled image pairs with the constraint that the interval between
 1127 two selected frames was at least ten frames. For the BridgeV2 dataset, we only considered videos
 1128 with four available perspectives and similarly enforced a minimum interval of ten frames between
 1129 sampled images. To ensure diversity, sampling was performed as evenly as possible across videos
 1130 and tasks.

1131 After this automatic step, each image pair was manually inspected by human annotators, and only
 1132 those judged suitable for QA were retained. At this stage, we obtained more than 3,000 high-
 1133 quality image pairs, which served as the foundation for constructing the benchmark. The perspective
 identification task required a different setup, and its details are described separately in Appendix C.



1134
1135

E.3 DEFINITION OF THE COORDINATE SYSTEM

1136
1137
1138

To ensure a consistent interpretation of spatial relations across different camera views, we define a standardized right-handed orthogonal coordinate system tied to each camera frame. The construction proceeds as follows:

1139
1140
1141

1. ***z*-axis (vertical).** Let \mathbf{g} denote the gravity vector, pointing downward. We define

1142
1143

$$\hat{\mathbf{z}} = -\frac{\mathbf{g}}{\|\mathbf{g}\|},$$

1144
1145

so that the $+z$ direction points upward (opposite to gravity) and $-z$ points downward.

1146
1147
1148

2. ***y*-axis (forward/backward).** Let \mathbf{c} denote the camera optical axis. Project \mathbf{c} onto the plane orthogonal to $\hat{\mathbf{z}}$:

1149

$$\mathbf{c}_\perp = \mathbf{c} - (\mathbf{c} \cdot \hat{\mathbf{z}})\hat{\mathbf{z}}.$$

1150
1151

Normalizing gives

1152
1153

$$\hat{\mathbf{y}} = \frac{\mathbf{c}_\perp}{\|\mathbf{c}_\perp\|},$$

1154
1155
1156

with orientation chosen so that the angle between $\hat{\mathbf{y}}$ and \mathbf{c} is strictly less than 90° . By convention, $+y$ corresponds to *forward*, while $-y$ corresponds to *backward*.

1157
1158

3. ***x*-axis (left/right).** Finally, the x -axis is determined by the right-hand rule:

1159
1160
1161

$$\hat{\mathbf{x}} = \hat{\mathbf{y}} \times \hat{\mathbf{z}}.$$

This ensures $+x$ points to the right side of the camera’s perspective and $-x$ to the left.

1162
1163
1164

Directional convention. In summary, $+z$ = upward, $-z$ = downward; $+y$ = forward, $-y$ = backward; $+x$ = right, $-x$ = left. Figure 12 provides an illustration of this definition.

1165
1166

E.4 TOOL FOR SPATIAL CUBE REASONING

1167
1168
1169
1170
1171

To construct the spatial cube reasoning task, we developed an interactive visualization tool that renders a standardized $5 \times 5 \times 5$ cube grid aligned with the camera coordinate system, where the x -, y -, and z -axes correspond to the *right*, *forward*, and *up* directions. Annotators can place colored unit cubes at integer grid coordinates, assign labels, and interactively edit or regenerate cube configurations.

1172
1173
1174
1175

This design enables rapid prototyping of spatial arrangements and provides a consistent interface for generating QA items that require reasoning about relative positions and geometric relationships in 3D space. The tool also supports keyboard-based coordinate input for efficient and reproducible annotation.

1176
1177

E.5 HUMAN ANNOTATION PROTOCOL AND QUALITY ASSURANCE

1178
1179
1180
1181

To ensure transparency in benchmark construction, we provide detailed information about the annotators, training procedures, human effort, and the quality-control pipeline adopted throughout the multi-stage annotation process.

1182
1183

E.5.1 ANNOTATOR TRAINING AND TASK UNDERSTANDING

1184
1185
1186
1187

All annotators participating in the construction of MV-RoboBench were senior undergraduate students or Ph.D. candidates in computer science or closely related fields. Before large-scale annotation began, we conducted a structured multi-stage training process to ensure that annotators had a rigorous understanding of the purpose and design philosophy of each subtask. First, for each subtask, we provided a conceptual overview explaining *why* the subtask was designed and *what specific*

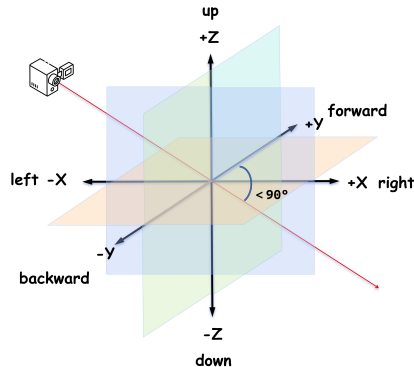


Figure 12: Illustration of the right-handed coordinate system defined relative to each camera.

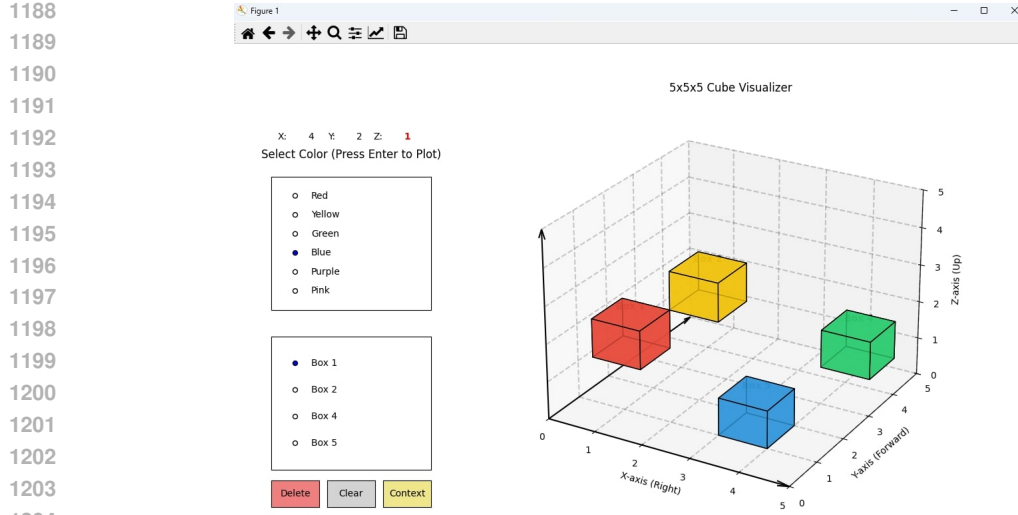


Figure 13: Screenshot of the spatial cube reasoning tool. Annotators can add, label, and manipulate colored cubes within a standardized $5 \times 5 \times 5$ grid to construct 3D reasoning problems.

aspect of multi-view robotic reasoning it aims to evaluate. For example, some subtasks target cross-view correspondence, others highlight 3D spatial understanding, action feasibility, or multi-step execution consistency. This high-level motivation helped annotators internalize the intended reasoning challenge behind each category rather than focusing solely on the mechanics of QA creation. Second, we supplied a curated set of high-quality QA examples for each subtask, including both well-constructed samples and typical failure cases. These examples illustrated desirable properties such as clear problem formulation, meaningful distractor design, and unambiguous ground-truth answers. Annotators were instructed to study these examples closely to understand how a robust QA item should be structured. Finally, annotators completed a trial stage in which they produced small batches of QA items. All trial results were reviewed individually by the authors, and detailed feedback was provided for every ambiguous, incorrect, or poorly structured item. Annotators revised their samples accordingly, and only after completing this iterative refinement stage were they allowed to contribute to the full annotation pipeline.

E.5.2 HUMAN EFFORT ESTIMATION

The construction of MV-RoboBench required substantial human effort across several stages of data preparation, annotation, and verification. We provide an estimate of the total annotation effort below. **Collection and Filtering of Image Pairs (~200 hours).** This stage involved selecting suitable datasets, writing scripts to automatically pre-filter candidate image pairs, and manually examining the automatically retrieved pairs to determine whether they exhibited clear multi-view correspondences appropriate for downstream QA construction. Annotators carefully removed pairs containing occlusions, poor synchronization, or ambiguous spatial relationships to ensure that only high-quality candidates entered the QA generation stage. **QA Construction and Iterative Refinement (~600 hours).** This stage accounted for the largest portion of the human effort. The workload included multiple rounds of internal discussion to finalize subtask definitions and question formats, training annotators on the annotation protocol, and iterative communication between authors and annotators to refine how each subtask should be expressed. The actual annotation time—spanning bounding-box drawing, spatial-cube configuration, distractor design, and multi-view reasoning checks—was intentionally left flexible to allow annotators to focus on ensuring that each QA item was both correct and diverse. **Cross-Checking and Validation (~400 hours).** After QA items were generated, multiple annotators independently reviewed all samples to identify ambiguous phrasing, weak distractors, or incorrect reasoning chains. Items flagged during this stage were either revised through further discussion or discarded entirely. This iterative multi-annotator cross-validation stage was critical for improving the reliability and robustness of the final benchmark.

1242 E.5.3 QUALITY-CONTROL PROCEDURES
1243

1244 Our benchmark follows the construction flow illustrated in Figure 2, but in this section we focus
 1245 specifically on the quality-control mechanisms incorporated into each stage rather than the pipeline
 1246 itself. The goal is to ensure that every QA item in MV-RoboBench is unambiguous, visually
 1247 grounded, and aligned with the intended reasoning challenge of its corresponding subtask. **Ini-**
 1248 **tial Image-Pair Screening.** Before any annotation begins, we employ a two-stage filtering process
 1249 to guarantee that only high-quality visual inputs enter the QA construction pipeline. First, we use
 1250 GPT-based filtering to select image-pair candidates that satisfy the definition of each subtask. Sec-
 1251 ond, trained annotators manually verify these candidates by checking whether the images exhibit
 1252 stable multi-view correspondences, sufficient visual clarity, and the absence of severe motion blur
 1253 or occlusion. Only pairs judged to be suitable for at least one subtask proceed to the annotation
 1254 stage. **Annotation with Structured Distractor Design.** After subtask definitions are finalized, an-
 1255 notators—who have undergone dedicated training (Section E.5.1)—construct QA items following
 1256 standardized guidelines. A critical aspect of our quality control is the design of distractors: each
 1257 question contains one correct answer and four distractors, among which annotators deliberately
 1258 create one or two *hard distractors* that closely resemble the correct answer, while the remaining
 1259 distractors are intentionally more distinct. This structure ensures both a meaningful level of dif-
 1260 ficulty and a clear separation between high-level reasoning errors and trivial misunderstandings.
 1261 During annotation, annotators also verify that the correct answer is uniquely supported by the vi-
 1262 sual evidence and that no distractor inadvertently becomes correct under alternative interpretations.
 1263 **Multi-Annotator Verification and Iterative Revision.** Once QA items are created, they are added
 1264 to a shared VQA pool and undergo multi-round cross-checking. Multiple annotators independently
 1265 review each sample. If *any* reviewer finds a QA item ambiguous, poorly structured, or misaligned
 1266 with the intended subtask, the item is immediately flagged. Flagged items are either revised through
 1267 further discussion—during which annotators and authors jointly inspect the visual evidence and rea-
 1268 soning steps—or discarded entirely. Revised items re-enter the VQA pool for additional rounds
 1269 of validation. This iterative process continues until all items satisfy strict correctness, clarity, and
 1270 reasoning requirements. Through this combination of automated pre-filtering, human verification,
 1271 structured annotation protocols, and multi-round cross-validation, MV-RoboBench achieves a high
 1272 degree of reliability and robustness across all subtasks.

1273 F DETAILS OF BENCHMARK CONSTRUCTION
1274

1275 In this appendix, we describe the construction details of each subtask included in our benchmark.
 1276 As introduced in Appendix E.2, we first obtained a large collection of high-quality image pairs
 1277 from AgiWorld and BridgeV2 through automatic sampling and manual filtering. These image pairs
 1278 serve as the common starting point for constructing the majority of subtasks, while the perspective
 1279 identification task required a different setup and is discussed separately later in this section.

1280 For clarity, we organize this appendix by task category. We first present the four **spatial** subtasks,
 1281 which focus on multi-view scene understanding: Cross-View Object Matching, Distance Judgement,
 1282 Viewpoint Identification, and 3D Spatial Consistency. We then describe the four **robotic** subtasks,
 1283 which extend spatial reasoning to manipulation scenarios: Action Planning, Step Execution, Trajec-
 1284 tory Selection, and Affordance Recognition. Finally, we conclude with a summary that highlights
 1285 the complementarity of these subtasks and provides an overview table (Table 6).

1286 F.1 CROSS-VIEW OBJECT MATCHING
1287

1288 This subtask belongs to the **spatial** category and evaluates whether a model can recognize the same
 1289 object across different camera viewpoints. In the construction process, one reference view is se-
 1290 lected, where the target object is highlighted with a red bounding box. In the remaining synchro-
 1291 nized views, candidate objects are marked with bounding boxes of different colors. The model is
 1292 then asked to identify which candidate corresponds to the same object as the red box in the reference
 1293 view.

1294 To avoid trivial solutions based only on object category or color cues, distractor candidates are
 1295 carefully chosen to be visually plausible. These include objects of the same category, those in

1296

1297

1298

1299

1300

1301

1302

1303

1304

1305

1306

1307

1308

1309

1310

1311

1312

1313

1314

1315

1316

1317

1318

1319

1320

1321

1322

1323

1324

1325

1326

1327

1328

1329

1330

1331

1332

1333

1334

1335

1336

1337

1338

1339

1340

1341

1342

1343

1344

1345

1346

1347

1348

1349



Template Cross-View Matching

In the **right-gripper** camera view, the **item** is outlined with a red bounding box. Which colored bounding box encloses that same item in the **left-gripper** camera view and the **head** camera view?

Rules

- You can replace the **orange nouns** with labeled objects, or you can just use **item** instead.
- You can replace the **right-gripper** with **left-gripper** or **head**
- The blue text is a template description, which can be copied directly.

Sample of Cross-View Matching



left gripper view

head view

right gripper view

Question: In the right-gripper camera view, the item is outlined with a red bounding box. Which colored bounding box encloses that same item in the left-gripper camera view and the head camera view?

OptionA: The blue bounding box.

OptionB: The green bounding box.

OptionC: The purple bounding box.

OptionD: The yellow bounding box.

OptionE: The pink bounding box.

Figure 14: Example of *Cross-View Object Matching* constructed from the AgiWorld dataset. The reference view marks the target with a red bounding box; other views contain color-coded candidate boxes, one of which corresponds to the ground-truth object.

close proximity, or partially overlapping instances, making the task a genuine test of cross-view association.

Figures 14 and 15 show representative examples of this subtask, constructed from the AgiWorld and BridgeV2 datasets, respectively.

F.2 DISTANCE JUDGEMENT

This subtask belongs to the **spatial** category and evaluates a model’s ability to reason about relative distances using synchronized multi-view observations. In each problem, one selected view presents several candidate objects, each marked with a colored bounding box. The model is asked to determine which candidate corresponds to the shortest (or, alternatively, the longest) grasping distance relative to the specified gripper. Other synchronized views provide additional context, requiring the model to integrate information across perspectives to resolve depth ambiguities.

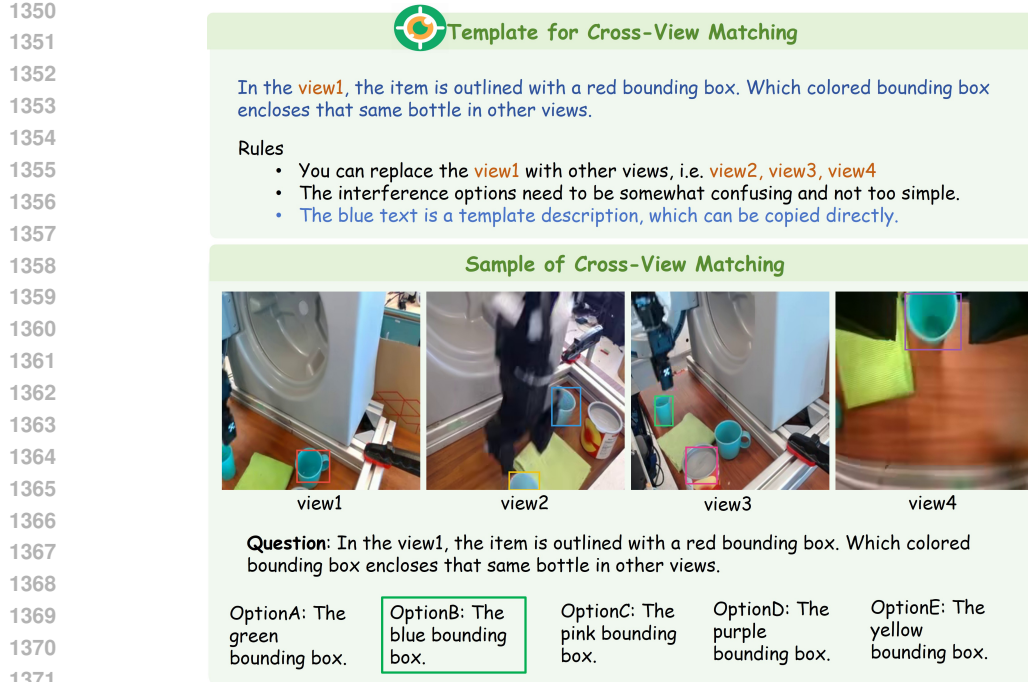


Figure 15: Example of *Cross-View Object Matching* constructed from the BridgeV2 dataset. The target is highlighted in view1, and the model must select the corresponding bounding box in the other synchronized views.

To ensure non-triviality, distractor options are manually verified so that objects with similar 2D appearances may differ in their actual 3D distances. Accurate solutions therefore demand reasoning that goes beyond single-view perception.

Figures 16 and 17 illustrate both representative instances and the annotation templates employed for constructing the *Distance Judgement* subtask in AgiWorld and BridgeV2.

F.3 VIEWPOINT IDENTIFICATION

This subtask belongs to the **spatial** category and evaluates a model’s ability to recognize and reason across different viewpoints. It is constructed exclusively from the AgiWorld dataset, where the reference image is always taken from the head camera. The question asks the model to determine which candidate image corresponds to the correct left- or right-gripper view at the same time step, given the head camera observation. Solving the task requires a form of perspective transformation, testing whether the model can imagine how the scene would appear from another viewpoint—a core component of spatial intelligence.

To construct distractor options, we adopt a multi-stage design. For each ground truth gripper image, we first include the image from the opposite gripper at the same time step. We then add distractors from the same episode but different time steps, ensuring a non-trivial temporal gap in the gripper poses so that the distractor cannot be rejected trivially. Additional distractors are sampled from other episodes within the same or closely related tasks, providing visually plausible but incorrect gripper views. This strategy prevents the model from exploiting majority-vote heuristics across options. All instances are manually verified to guarantee that a human annotator can reliably identify the correct correspondence based on spatial details.

Figure 18 illustrates both the template and an example instance of this subtask.

1404

1405

1406

1407

1408

1409

1410

1411

1412

1413

1414

1415

1416

1417

1418

1419

1420

1421

1422

1423

1424

1425

1426

1427

1428

1429

1430

1431

1432

1433

1434

1435

1436

1437

1438

1439

1440

1441

1442

F.4 3D SPATIAL CONSISTENCY

This subtask is part of the **spatial** category and evaluates a model’s ability to reason about object locations within a structured 3D coordinate system. The key challenge is to assess whether the model can treat the scene as a three-dimensional space rather than a flat image, and correctly place the highlighted objects into the standardized coordinate grid such that their relative positions remain coherent across views.

We adopt a right-handed orthogonal coordinate system anchored to a designated reference view (the head camera in AgiWorld, or any of the four views in BridgeV2). In the reference image, several target objects are highlighted with colored bounding boxes. The question then asks the model: “*Which of the following sets of coordinate triplets best describes the positions of the highlighted objects?*” Coordinates are normalized into a $5 \times 5 \times 5$ cubic grid, with integer values from 1 to 5 along each axis. This abstraction allows spatial relations to be expressed consistently without requiring precise metric depth.

 **Template for Distance Judgement**

You are given three synchronized views—the left-gripper camera, the head camera, and the right-gripper camera. Only the head camera image contains colored bounding boxes. Which option corresponds to the **shortest** grasping distance?

Rules

- The orange box is a good interference option because there is depth ambiguity in the head camera view.
- You can replace the **shortest** with **longest**.
- The blue text is a template description, which can be copied directly.

Sample of Distance Judgement



left gripper view



head view



right gripper view

Question: You are given three synchronized views—the left-gripper camera, the head camera, and the right-gripper camera. Only the head camera image contains a colored bounding box. Which option corresponds to the shortest grasping distance?

OptionA: Grab the item in the green bounding box using the left gripper.	OptionB: Grab the item in the yellow bounding box using the left gripper.	OptionC: Grab the item in the yellow bounding box using the right gripper.	OptionD: Grab the item in the yellow bounding box using the right gripper.
		OptionE: Grab the item in the yellow bounding box using the right gripper.	

Figure 16: Example of *Distance Comparison* constructed from the AgiWorld dataset. The head camera image contains candidate bounding boxes, and the model must select the one corresponding to the shortest grasping distance.

27

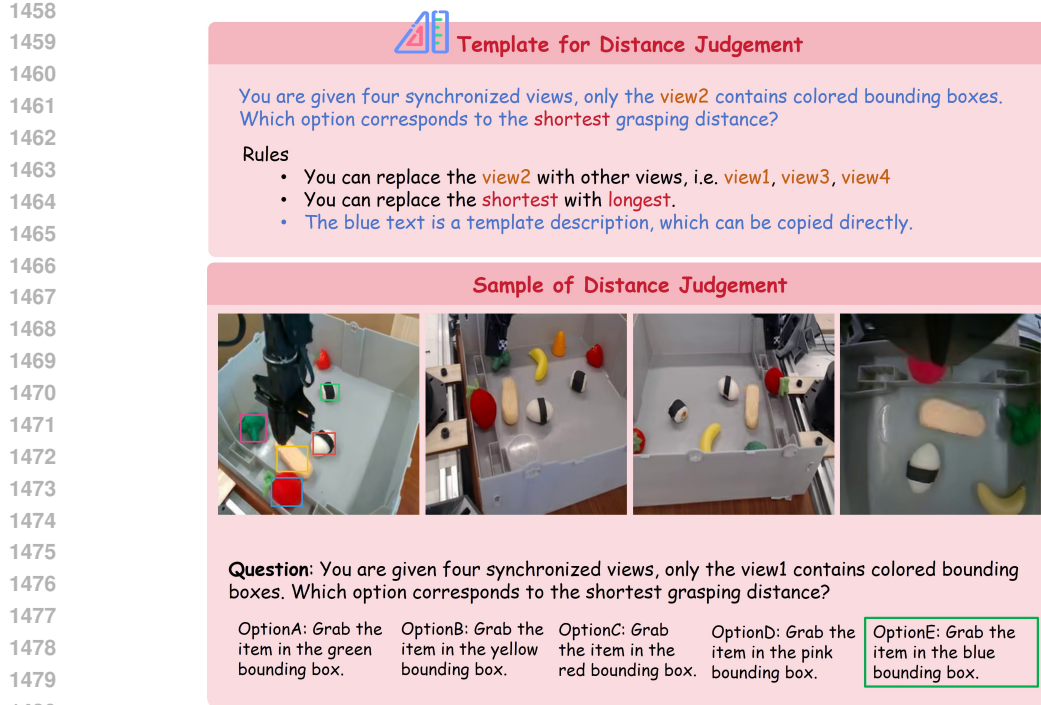


Figure 17: Example of *Distance Comparison* constructed from the BridgeV2 dataset. One view contains candidate bounding boxes, and the model must identify the option that corresponds to the shortest grasping distance when integrating evidence across all four views.

To construct the tasks, we leverage the interactive cube visualization tool described in Appendix E.4. This tool enables annotators to map each object to a unit cube in the grid, adjust placements, and generate candidate coordinate sets. Distractor options are created by perturbing object coordinates to introduce plausible but incorrect spatial configurations. Accurate solutions therefore require integrating multi-view cues rather than relying on a single perspective.

Figures 19 and 20 show representative templates and examples constructed from the AgiWorld and BridgeV2 datasets, respectively.

F.5 ACTION PLANNING

This subtask belongs to the **robotic** category and evaluates whether a model can correctly identify the valid high-level action sequence from multiple candidates in order to accomplish a manipulation goal. Each instance provides synchronized multi-view observations together with a task description in natural language. The problem is defined with respect to a designated reference view, within which we establish the standardized right-handed coordinate system described in Appendix E.3. Accordingly, all candidate action sequences are expressed as sequences of normalized directional terms (i.e., spatial adverbs such as *leftward*, *forward*, *downward*), which follow directly from the axis conventions defined in Appendix E.3. The model must then integrate information across views and select the sequence most likely to achieve the goal.

To ensure non-triviality, distractor options are carefully constructed. Only one option corresponds to a valid sequence that completes the task while minimizing collisions, whereas the distractors follow plausible but incorrect paths. In addition, we enumerate and sort the directional terms within each option, ensuring that no two candidates share the same ordered sequence of actions. This design prevents ambiguity and forces the model to reason jointly about spatial relations and manipulation feasibility.

Figures 21 and 22 illustrate representative templates and examples from the AgiWorld and BridgeV2 datasets, respectively.

1512

1513

1514

1515

1516

1517

1518

1519

1520

1521

1522

1523

1524

1525

1526

1527

1528

1529

1530

1531

1532

1533

1534

1535

1536

1537

1538

1539

1540

1541

1542

1543

1544

1545

1546

1547

1548

1549

1550

1551

1552

1553

1554

1555

1556

1557

1558

1559

1560

 **Template for Viewpoint Identification**

Given the image captured by the head camera, which of the following images shows the **right-gripper** camera's view at that exact moment?

Rules

- You can replace the **right-gripper** with **left-gripper**.
- The blue text is a template description, which can be copied directly.

Sample for Viewpoint Identification



OptionA: Option A picture.



OptionB: Option B picture.



OptionC: Option C picture.



OptionD: Option D picture.



OptionE: Option E picture.

Figure 18: Example of *Perspective Identification* constructed from the AgiWorld dataset. The head camera view is used as the reference, and the model must infer the correct corresponding perspective among the candidate gripper views.

F.6 STEP EXECUTION

This subtask belongs to the **robotic** category and focuses on low-level action execution in manipulation tasks. Each instance provides synchronized multi-view observations together with a natural language description of the goal. Unlike the *Action Planning* task, which evaluates multi-step trajectories, *Step Execution* concentrates on primitive actions such as picking or placing, which can be described as short sequences of directional terms (e.g., *up*, *left*, *down*). The coordinate system is defined with respect to a designated reference view, following the conventions introduced in Ap-

1566 pendix E.3. All candidate options are then expressed in these normalized directional terms, and the
 1567 model must select the sequence that correctly achieves the task.
 1568

1569 Distractor options are constructed to appear plausible but correspond to incorrect motions that would
 1570 fail the manipulation. To eliminate redundancy, we further enumerate and sort the directional terms
 1571 within each option, ensuring that no two candidates reduce to the same ordered sequence. This
 1572 design requires the model to interpret spatial cues accurately across multiple views and to ground its
 1573 decision in the standardized coordinate system. For the AgiWorld dataset, the template is based on
 1574 synchronized left-gripper, head, and right-gripper views, while in BridgeV2 any of the four available
 1575 views may serve as the reference.
 1576

1577 Figures 23 and 24 show representative templates and examples from the AgiWorld and BridgeV2
 1578 datasets, respectively.
 1579

1580 F.7 TRAJECTORY SELECTION

1581
 1582 This subtask belongs to the **robotic** category and evaluates a model’s ability to reason about com-
 1583 plete motion trajectories in multi-view settings. Each instance provides synchronized observations,
 1584 where candidate trajectories are overlaid in different colors on one or more reference views. The
 1585 model is asked to determine which trajectory is most likely to accomplish the described manipula-
 1586 tion.

1587 A key challenge is that trajectories drawn in a single view may be ambiguous due to occlusions,
 1588 perspective distortion, or motion along the camera’s optical axis. By providing multiple synchro-
 1589 nized viewpoints, the task requires the model to integrate cross-view evidence to correctly identify
 1590 the feasible trajectory.

1591 All distractor trajectories are *manually curated* to be distinct from the ground truth yet visually plau-
 1592 sible, so that they may appear confusing at first glance but remain distinguishable through careful
 1593 multi-view reasoning. We ensure that exactly one candidate is feasible across views and can com-
 1594 plete the task without collisions; every instance is human-validated to confirm that the correct choice
 1595 is uniquely identifiable.

1596 For the AgiWorld dataset, each problem is presented with synchronized left-gripper, head, and right-
 1597 gripper views. For BridgeV2, all four camera perspectives are available, and candidate trajectories
 1598 are described relative to these views. Figures 25 and 26 provide representative templates and exam-
 1599 ples from both datasets.
 1600

1601 F.8 AFFORDANCE RECOGNITION

1602
 1603 This subtask belongs to the **robotic** category and evaluates a model’s ability to recognize feasible
 1604 grasp candidates in multi-view scenes. In real manipulation, a single viewpoint may be insufficient
 1605 for identifying good grasp locations due to occlusions by objects or grippers, or because certain
 1606 camera angles (e.g., top-down) obscure critical contact geometry. By incorporating synchronized
 1607 multi-view observations, especially from gripper-mounted cameras, this task provides complemen-
 1608 tary perspectives that make the final grasp point more reliably observable.
 1609

1610 Each instance presents five candidate grasps illustrated with color-coded lines (red, yellow, green,
 1611 blue, and pink). Each color appears exactly once across the available views, and the two endpoints of
 1612 a line specify the intended positions of the gripper fingers. The model is asked: “*Which color-coded*
 1613 *line represents the grasp candidate most likely to succeed?*”
 1614

1615 All distractors are carefully designed: while they may appear physically plausible at first glance, they
 1616 are infeasible in practice due to orientation, collision risk, or instability. This ensures that success
 1617 requires genuine spatial reasoning and affordance understanding rather than superficial cues. For
 1618 the AgiWorld dataset, three views (left-gripper, head, right-gripper) are used, whereas in BridgeV2
 1619 the template extends naturally to four synchronized views. Figures 27 and 28 provide representative
 1620 templates and examples from both datasets.

1620 Table 6: Overview of the eight subtasks in our benchmark. Spatial tasks focus on multi-view scene
 1621 understanding, while robotic tasks extend this foundation to manipulation planning and execution.
 1622

Category	Subtask	Core Ability Assessed
Spatial	Cross-View Object Matching	Identify the same object across different viewpoints despite distractors.
	Distance Judgement	Compare relative distances to a specified gripper using multi-view cues.
	Viewpoint Identification	Infer the correct camera perspective given a head-view reference.
	3D Spatial Consistency	Place highlighted objects into a structured 3D coordinate system with coherent relative positions.
Robotic	Action Planning	Select the valid high-level action sequence in normalized directional terms to accomplish a task.
	Step Execution	Choose the correct primitive low-level action sequence (e.g., pick/place) grounded in the coordinate system.
	Trajectory Selection	Distinguish feasible from infeasible motion trajectories by integrating evidence across views.
	Affordance Recognition	Identify the grasp candidate most likely to succeed among visually plausible alternatives.

1635 F.9 ANSWER BALANCING AND RANDOMIZATION

1637 After generating QA instances and completing manual verification, we apply an additional balancing
 1638 step to ensure that answer distributions are statistically uniform. Specifically, correct answers are
 1639 randomized across different option indices and color assignments, preventing systematic biases that
 1640 could allow models to exploit position- or color-based heuristics. This balancing guarantees that
 1641 success on the benchmark requires genuine spatial reasoning and affordance understanding rather
 1642 than relying on superficial answer patterns.

1643 F.10 SUMMARY OF BENCHMARK CONSTRUCTION

1645 Taken together, the eight subtasks provide a comprehensive evaluation of spatial and robotic reasoning
 1646 in multi-view environments.

1648 The four **robotic** subtasks (Action Planning, Step Execution, Trajectory Selection, and Affordance
 1649 Recognition) extend this foundation to manipulation scenarios. They examine whether models can
 1650 ground spatial understanding into action decisions, ranging from high-level planning to low-level ex-
 1651 ecution, and from trajectory-level reasoning to grasp affordance prediction. Together, they highlight
 1652 the importance of combining multi-view perception with physical feasibility in order to succeed in
 1653 robotic tasks.

1654 An overview of all subtasks, their categories, and the specific reasoning abilities they target is pro-
 1655 vided in Table 6.

1657 G ABLATION STUDY ON MULTI-VIEW NECESSITY

1659 In this section, we address the fundamental question of whether multi-view inputs are truly necessary
 1660 for the proposed robotic reasoning tasks, or if a single-view input would suffice. To investigate this,
 1661 we conducted a systematic ablation study comparing the performance of representative models under
 1662 a **Single-View** baseline versus the standard **Multi-View** setting.

1664 G.1 TASK SELECTION AND EXPERIMENTAL SETUP

1665 Our benchmark consists of eight subtasks. However, not all tasks are suitable for single-view eval-
 1666 uation due to their inherent reliance on cross-view information. We applied the following selection
 1667 criteria:

- 1669 • **Excluded Tasks (Inherently Multi-View):** For subtasks including *Cross-View Object*
 1670 *Matching*, *Viewpoint Identification*, *Trajectory Selection*, and *Affordance Recognition*, the
 1671 question semantics inherently depend on multiple synchronized views. Many answer can-
 1672 didates exist only in specific views, so removing views would yield ill-posed questions
 1673 (e.g., some candidates become invisible). Therefore, these tasks were excluded from the
 1674 ablation.

1674
 1675
 1676
 1677
 1678
 1679
 1680
 1681
 1682
 1683
 1684
 1685
 1686
 1687
 1688
 1689
 1690
 1691
 1692
 1693
 1694
 1695
 1696
 1697
 1698
 1699
 1700
 1701
 1702
 1703
 1704
 1705
 1706
 1707
 1708
 1709
 1710
 1711
 1712
 1713
 1714
 1715
 1716
 1717
 1718
 1719
 1720
 1721
 1722
 1723
 1724
 1725
 1726
 1727

- **Selected Tasks (Degradable to Single-View):** We focused our ablation on the remaining four subtasks: *Distance Judgement*, *3D Spatial Consistency*, *Action Planning*, and *Step Execution*. These tasks are typically formulated relative to a reference coordinate system or a primary scene description. While multi-view information provides critical depth cues and occlusion handling, these questions remain logically valid even when restricted to a single input image. This allows us to rigorously measure the “performance drop” caused by the loss of multi-view context.

For the **Single-View** setting, we retained only the most informative third-person perspective to ensure a strong baseline:

- For the **AgiWorld** dataset, we used the *head camera* view.
- For the **BridgeV2** dataset, we used *view1* (a fixed third-person camera).

G.2 RESULTS AND ANALYSIS

Table 7 presents the comparative results. We report the full multi-view accuracy and the performance gap (Δ) relative to the single-view baseline.

Table 7: Comparison of Single-View vs. Multi-View performance on selected subtasks. The values represent Multi-View accuracy, and values in parentheses indicate the change (Δ) compared to the Single-View baseline. Positive Δ indicates that multi-view inputs improve performance. **Bold** indicates the best performance in each category.

Model	Avg.	Distance Judge.	3D Spatial Cons.	Action Plan.	Step Exec.
<i>Proprietary Reasoning Models</i>					
GPT-5	64.65 (+6.69)	36.32 (+18.90)	78.43 (+3.92)	76.96 (+2.45)	66.24 (+2.14)
GPT-5-chat	28.11 (+3.05)	29.35 (+13.44)	10.29 (-5.39)	35.29 (+1.47)	36.32 (+3.85)
<i>Proprietary Models</i>					
GPT-4.1	24.20 (+3.59)	32.84 (+10.44)	4.90 (+1.47)	30.39 (-0.49)	28.21 (+3.41)
GPT-4o	26.81 (+0.88)	31.84 (+5.47)	5.39 (+0.98)	33.82 (-0.49)	35.04 (-1.28)
<i>Open-Source Models</i>					
Qwen2.5-vl-72b	23.01 (+0.87)	30.85 (+3.98)	3.92 (+0.98)	30.88 (-2.45)	26.07 (+1.28)
Qwen2.5-vl-32b	20.28 (-0.07)	24.38 (+1.49)	8.33 (+2.45)	25.49 (-1.98)	22.65 (-2.99)
Qwen2.5-vl-7b	17.91 (+1.55)	20.40 (0.00)	4.90 (+3.92)	21.08 (+1.47)	24.36 (+1.71)

Our analysis yields three key findings regarding the necessity of multi-view perception:

1. **Multi-view is critical for resolving spatial ambiguity.** The most significant impact is observed in the *Distance Judgement* task. Powerful reasoning models like GPT-5 and GPT-4.1 achieve substantial gains (+18.90% and +10.44%, respectively) when provided with multi-view inputs. This confirms that single-view observations suffer from inherent depth ambiguity and occlusion—common issues in robotic manipulation—which are effectively mitigated by integrating complementary viewpoints.
2. **Stronger reasoning capabilities unlock multi-view potential.** We observe a positive correlation between model capability and the benefit derived from multi-view information. State-of-the-art models consistently improve with additional views, whereas smaller models (e.g., Qwen2.5-vl-32b, Qwen2.5-vl-7b) show negligible or even negative changes. This suggests that effectively fusing discordant visual information requires strong spatial reasoning capabilities; without this, smaller models may be distracted by the increased visual context rather than aided by it.
3. **Performance gap remains significant.** Even with the advantage of multi-view inputs, the performance on robotic planning tasks generally lags behind human proficiency. This highlights that while multi-view input is a necessary condition for robust perception, it is not sufficient on its own. Future models must develop stronger embodied reasoning capabilities to fully leverage the rich 3D information provided by MV-RoboBench.

H. IMPACT OF IMAGE ORIENTATION ON SPATIAL REASONING

To evaluate the generalization capabilities of VLMs regarding image orientation, we conducted an additional stress test. In this experiment, we vertically flipped **all camera views except for the gripper-mounted ones** (e.g., the head camera in AgiWorld and all static third-person views in BridgeV2) upside down. This setup disrupts the canonical spatial structure (e.g., visual “up” no longer aligns with gravity) without altering the intrinsic object relationships.

Crucially, this manipulation does not affect the correctness of the ground truth answers. As defined in Appendix E.3, our coordinate systems are established based on the physical gravity vector (g) and the camera’s optical axis (c), rather than the 2D image pixel axes. Since the physical scene configuration and sensor properties remain unchanged, the logical spatial relationships (e.g., “left”, “up”, “forward”) remain valid. Therefore, any performance drop can be attributed solely to the models’ inability to generalize to non-canonical visual orientations.

Table 8 reports the detailed performance under this upside-down setting across all subtasks.

Table 8: Detailed performance under Upside-Down image orientation. “Avg” represents the average accuracy in the upside-down setting. “ Δ ” denotes the performance drop compared to the original setting. The remaining columns show the specific accuracy for each subtask under the upside-down condition.

Model	Avg	Δ	Spatial Tasks				Robotic Tasks			
			Cross	Dist.	View.	3D Cons.	Plan	Step	Traj.	Afford.
<i>Proprietary Reasoning Models</i>										
GPT-5	37.68	-18.73	33.50	30.35	25.00	26.47	47.55	40.60	53.50	44.50
GPT-5-mini	30.79	-7.49	31.50	23.88	21.88	17.16	46.57	38.89	42.50	23.92
GPT-5-nano	22.42	-10.33	17.00	18.41	22.66	11.76	28.43	25.21	30.50	25.36
GPT-5-chat	28.50	-3.13	31.00	35.32	27.34	6.37	33.33	33.76	35.50	25.36
<i>Proprietary Models</i>										
GPT-4.1	26.72	-4.18	26.50	33.33	33.59	4.90	27.94	29.49	37.00	21.05
GPT-4o	25.10	-2.49	25.50	31.84	23.44	4.90	30.39	31.20	33.00	20.57
GPT-4.1-mini	23.94	-0.04	22.50	26.37	27.73	6.37	25.98	25.21	32.50	24.88
GPT-4.1-nano	20.08	-0.77	17.50	16.42	18.36	12.25	25.98	25.21	20.00	24.88
<i>Open-Source Models</i>										
Qwen2.5-vl-72b	23.33	-0.96	23.50	23.88	22.27	3.92	28.92	27.35	29.50	27.27
Qwen2.5-vl-32b	22.41	-0.07	24.50	28.86	23.05	3.92	25.00	23.93	28.50	21.53
Qwen2.5-vl-7b	19.71	-1.13	22.00	20.90	20.31	5.39	23.04	26.50	19.00	20.57

We observe distinct behaviors across model families:

1. **Strong models exhibit strong orientation bias.** The most capable model, GPT-5, suffers the largest performance drop ($\Delta = -18.73\%$). Comparing this to its baseline performance in Table 2, we see a dramatic decline in *3D Spatial Consistency* (from 82.35% to 26.47%) and *Distance Judgement* (from 55.22% to 30.35%). This indicates that its superior spatial reasoning capabilities rely heavily on the canonical “upright” orientation learned during pre-training. When the visual reference frame is inverted, the model struggles to maintain coherent 3D spatial relations.
2. **Weaker models show a floor effect.** In contrast, smaller models (e.g., GPT-4.1-mini, Qwen2.5-vl-7b) show negligible performance changes ($\Delta \approx 0$). As shown in Table 2, these models already perform poorly on spatial tasks in the standard setting (e.g., $\sim 7\text{-}9\%$ on *3D Spatial Consistency*). This confirms that their original performance was likely dominated by pattern matching or random guessing rather than genuine spatial understanding, making them insensitive to orientation flips.
3. **Implications for deployment.** While this result highlights a limitation in zero-shot generalization, we note that in real-world robotic deployment, camera mounting poses are strictly controlled, and input images are typically inspected or rectified to ensure a canonical orientation. Therefore, while VLMs lack rotation invariance, this sensitivity is a manageable characteristic in engineered systems.

1782 I EVALUATION OF MODEL CAPABILITY TO REJECT INCORRECT OPTIONS 1783

1784 The ability to determine when no correct answer exists is critical for safe robotic deployment. As
1785 pointed out by the reviewers, evaluating this "rejection" capability is a vital aspect of spatial reason-
1786 ing.

1787 In our original benchmark design, we partially incorporated this dimension. Specifically, in the
1788 *Cross-View Object Matching* task, approximately 25% of the questions explicitly include a ground-
1789 truth option of "None of the bounding boxes is correct." This was designed to prevent models from
1790 relying solely on elimination.

1791 However, to provide a more comprehensive and extreme evaluation of this capability across the
1792 entire benchmark, we conducted a controlled stress test on 7 out of the 8 subtasks.

1794 I.1 EXPERIMENTAL SETUP

1796 We modified the dataset by replacing the original ground-truth option with "None of the above" for
1797 every question in the selected subtasks. The original correct answer was removed, making "None
1798 of the above" the only valid choice. To avoid positional bias, we ensured this option appeared as
1799 option E.

1800 **Exclusion of Distance Judgement:** We excluded the *Distance Judgement* task from this specific
1801 ablation. In this task, questions ask for the "shortest" or "longest" distance among candidates.
1802 Removing the absolute shortest candidate would logically make the *second* shortest candidate the
1803 new correct answer, creating ambiguity rather than a clear "None of the above" scenario. All other
1804 7 subtasks allow for a binary valid/invalid distinction, making them suitable for this test.

1806 I.2 RESULTS AND ANALYSIS

1808 Table 9 presents the results. We report the accuracy when the correct answer is "None of the above"
1809 (Reject. Avg.) and the performance drop compared to the standard setting.

1810 Table 9: Model performance on the "None of the above" rejection test. "**Reject.**" denotes the
1811 accuracy on the modified dataset where the correct answer is "None of the above". "**Drop**" indicates
1812 the performance decline relative to the original benchmark accuracy. A significant drop implies high
1813 model over-compliance.

Model	Reject.	Drop	Spatial Tasks			Robotic Tasks			Affordance Rec.
	Avg.		Cross-View Match	Viewpoint ID	3D Spatial Consist.	Action Plan.	Step Exec.	Trajectory Sel.	
<i>Proprietary Reasoning Models</i>									
GPT-5	13.43	-43.29	29.00	6.64	6.37	23.04	20.09	6.00	2.87
GPT-5-mini	9.57	-34.71	26.00	0.39	9.80	8.33	20.09	0.50	1.91
GPT-5-chat	1.05	-28.84	1.50	1.95	1.47	0.98	0.43	1.00	0.00
GPT-5-nano	8.61	-24.02	21.00	5.08	16.18	2.94	7.26	3.50	4.31
<i>Proprietary Models</i>									
GPT-4.1	0.60	-27.35	1.50	0.78	0.98	0.49	0.43	0.00	0.00
GPT-4.1-mini	3.74	-19.09	3.00	1.95	1.47	3.92	15.81	0.00	0.00
GPT-4.1-nano	0.78	-18.21	0.00	0.00	0.00	0.00	2.56	0.50	2.39
GPT-4o	0.92	-23.51	1.50	3.12	0.49	0.00	0.85	0.50	0.00
<i>Open-Source Models</i>									
Qwen2.5-vl-72b	3.39	-19.81	9.00	0.78	8.82	1.96	1.71	1.00	0.48
Qwen2.5-vl-7b	0.49	-20.31	2.00	0.00	0.98	0.00	0.00	0.00	0.48
Qwen2.5-vl-32b	0.28	-21.70	1.00	0.00	0.49	0.00	0.00	0.00	0.48

1829 The results reveal a severe "Over-Compliance" phenomenon across all models:

- 1831 1. **Universal collapse in rejection capability.** Even the strongest model, GPT-5, drops from
1832 56% accuracy to 13% when forced to reject incorrect options. Most other models collapse
1833 to near 0%, indicating they almost always hallucinate a relationship or force a selection
1834 from the visual candidates rather than acknowledging the absence of a correct answer.
- 1835 2. **Selection bias dominates validity judgement.** The experiment demonstrates that current
1836 models exhibit a strong tendency to select a "visually approximate" option rather than re-

1836jecting all options. Choosing “None of the above” imposes a higher cognitive requirement:
 1837 the model must distinguish between “relative similarity” and “absolute correctness,” and
 1838 possess an internal standard of rationality to invalidate all candidates. The results con-
 1839 firm that even advanced reasoning models currently struggle with this rigorous verification,
 1840 preferring to conform to the prompt by picking a plausible-looking but incorrect answer.

1841 3. **Implication.** This experiment highlights a critical safety gap in current VLM technology.
 1842 While models can reason about what is present, they struggle significantly to verify cor-
 1843 rectness by rejecting invalid options. MV-RoboBench effectively exposes this limitation,
 1844 serving as a testbed for future work on uncertainty estimation and refusal.

1846 J ERROR ANALYSIS OF MODEL FAILURES

1848 To better understand how current models fail on MV-RoboBench, we conduct a qualitative error
 1849 analysis on three representative models: a strong proprietary model (GPT-5), a strong open model
 1850 (Qwen2.5-VL-72B-Instruct), and a weaker open model (Qwen2.5-VL-7B-Instruct). For each model,
 1851 we sample 10–20 erroneous cases from several core subtask families, and manually inspect their
 1852 predictions and explanations. Below we summarize the main recurring failure modes and highlight
 1853 representative examples.

1855 **Single-view bias and weak multi-view fusion.** Across all three models, a prominent failure mode
 1856 is an over-reliance on a single camera view while largely ignoring contradictory evidence from
 1857 other views. GPT-5, for instance, often selects the option that looks most natural in the head view
 1858 but becomes inconsistent once the gripper views are taken into account. Qwen2.5-VL-7B shows
 1859 an even stronger single-view bias in cross-view matching and distance judgment tasks, where it
 1860 tends to align 2D screen positions across cameras (e.g., “bottom-right” to “bottom-right”) instead of
 1861 reasoning in a shared 3D frame. Qwen2.5-VL-72B behaves similarly in viewpoint identification and
 1862 cross-view tasks, effectively treating them as single-image retrieval problems rather than enforcing
 1863 multi-view geometric consistency.

1864 **Depth, occlusion, and 3D geometry confusion.** A second common failure mode involves incor-
 1865 rect reasoning about depth, occlusion, and 3D layout. In GPT-5, distance judgment and 3D spatial
 1866 consistency errors show that the model frequently substitutes 2D heuristics (apparent size, 2D po-
 1867 sition) for true 3D reasoning: it chooses objects that appear more salient or closer in a single pro-
 1868 jection, even when other views clearly indicate that another object is nearer in 3D. Qwen2.5-VL-7B
 1869 exhibits even stronger depth confusion, sometimes inverting near-far or front-back relations, and
 1870 occasionally treating objects on the tabletop and objects below the table (e.g., cabinet handles) as
 1871 comparable candidates. Qwen2.5-VL-72B shows similar issues in fine-grained 3D spatial consis-
 1872 tency, where it misassigns grid coordinates along the depth axis or swaps two neighboring objects
 1873 that are close in distance. These patterns suggest that current models lack robust internal 3D scene
 1874 representations and often rely on weak perspective cues.

1875 **Frame-of-reference errors and instance-level correspondence.** Even with an explicitly defined
 1876 camera-centric coordinate system (Appendix E.3), models often mishandle frame-of-reference de-
 1877 tails and instance-level matching. For GPT-5, viewpoint identification and cross-view matching
 1878 failures indicate that the model sometimes implicitly assumes that the same set of objects must
 1879 be visible in all views, and treats changes in visibility due to field-of-view or occlusion as evi-
 1880 dence that the views are asynchronous or unrelated. For Qwen2.5-VL-7B, we frequently observe
 1881 instance-level confusion in scenes with multiple objects of the same category (e.g., several yellow
 1882 peppers): the model correctly recognizes the category but fails to track which specific instance
 1883 is highlighted across views, effectively performing category-level rather than instance-level corre-
 1884 spondence. Qwen2.5-VL-72B exhibits similar behavior in multi-object setups, where it matches
 1885 “any object of the correct type” instead of the exact instance indicated by the bounding box. These
 1886 errors highlight the difficulty of precise, instance-level multi-view alignment even for large models.

1887 **Affordance and physical-feasibility misunderstandings.** In affordance recognition and trajec-
 1888 tory selection tasks, models must reason about which grasps or motion paths are more likely to

1890 succeed physically. GPT-5 often prefers grasp lines or trajectories that look visually neat (e.g., centered on the visible surface) but would be unstable or collision-prone for a parallel gripper in 3D; it
1891 rarely reasons explicitly about approach direction, object thickness, or nearby obstacles. Qwen2.5-
1892 VL-7B sometimes mislocalizes the grasp line to the wrong object altogether and then optimizes
1893 within this incorrect frame, leading to explanations that sound plausible but are grounded in the
1894 wrong spatial reference. Qwen2.5-VL-72B exhibits related issues: it often treats “passing through
1895 the middle” as a universal heuristic for good paths, even when the task requires side grasps on thin
1896 objects or collision-aware trajectories that avoid table edges and surrounding clutter. Overall, these
1897 failures indicate that current VLMs still lack robust modeling of robotic affordances and physical
1898 constraints, especially when such reasoning must be carried out jointly with multi-view geometric
1899 alignment.
1900

1901 **Summary.** Importantly, these failure modes appear not only in weaker models but also in GPT-
1902 5, which still exhibits systematic errors in multi-view fusion, depth reasoning, frame-of-reference
1903 handling, and affordance understanding. This suggests that MV-RoboBench does not merely lower
1904 raw accuracy; it exposes non-trivial limitations in current vision–language models’ spatial reasoning,
1905 and can serve as a diagnostic tool for guiding future architectural and training improvements.
1906
1907
1908
1909
1910
1911
1912
1913
1914
1915
1916
1917
1918
1919
1920
1921
1922
1923
1924
1925
1926
1927
1928
1929
1930
1931
1932
1933
1934
1935
1936
1937
1938
1939
1940
1941
1942
1943

1944
1945
1946
1947
1948
1949
1950
1951
1952
1953
1954
1955
1956



Template for 3D Spatial Consistency

You are given three synchronized views—the left-gripper camera, the head camera, and the right-gripper camera. Only the head camera image contains colored bounding boxes. Then assuming the workspace is divided into a $5 \times 5 \times 5$ cubic grid, with coordinates (x, y, z) running from 1 to 5. Which of the following sets of coordinate triplets best describes the locations of the objects circled by the bounding boxes in the image above? The following options are based on the head camera view. + <Description of coordinate system definition>

Rules

- The blue text is a template description, which can be copied directly.

Sample of 3D Spatial Consistency

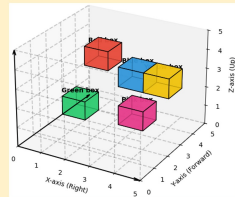


left gripper view

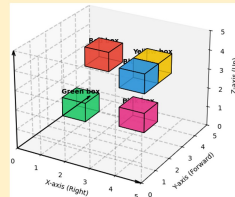
head view

right gripper view

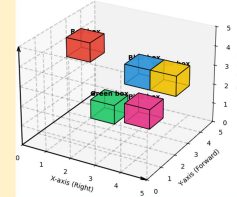
Question: As shown above



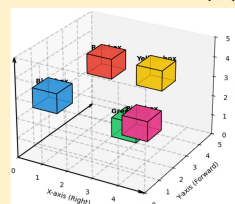
OptionA: (Red box, 2, 4, 4), (Yellow box, 5, 3, 4), (Green box, 1, 4, 1), (Blue box, 4, 3, 4), (Pink box, 4, 3, 2)



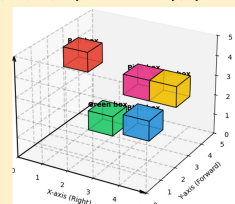
OptionB: (Red box, 2, 4, 4), (Yellow box, 4, 4, 4), (Green box, 1, 4, 1), (Blue box, 4, 3, 4), (Pink box, 4, 3, 2)



OptionC: (Red box, 1, 4, 4), (Yellow box, 5, 3, 4), (Green box, 2, 4, 1), (Blue box, 4, 3, 4), (Pink box, 4, 3, 2)



OptionD: (Red box, 2, 4, 4), (Yellow box, 4, 4, 4), (Green box, 3, 4, 1), (Blue box, 1, 2, 3), (Pink box, 4, 3, 2)



OptionE: (Red box, 1, 4, 4), (Yellow box, 5, 3, 4), (Green box, 2, 4, 1), (Blue box, 4, 3, 2), (Pink box, 4, 3, 4)

1990
1991
1992
1993
1994
1995
1996
1997

Figure 19: Example of *Spatial Cube Reasoning* from the AgiWorld dataset. Objects are localized in a $5 \times 5 \times 5$ cubic grid, and the model must select the correct coordinate triplets from the given options.

1998
1999
2000
2001
2002
2003
2004
2005
2006  **Template for 3D Spatial Consistency**
2007
2008
2009
2010
2011
2012
2013
2014
2015
2016
2017
2018
2019
2020
2021
2022
2023
2024
2025
2026
2027
2028
2029
2030
2031
2032
2033
2034
2035
2036
2037
2038
2039
2040
2041
2042
2043
2044
2045
2046
2047
2048
2049
2050
2051

You are given four synchronized views, only the **view1** contains colored bounding boxes. Then assuming the workspace is divided into a $5 \times 5 \times 5$ cubic grid, with coordinates (x, y, z) running from 1 to 5. Which of the following sets of coordinate triplets best describes the locations of the objects circled by the bounding boxes in the image above? The following options are based on the **view1**. <Description of coordinate system definition>

Rules

- You can replace the **view1** with other views, i.e. **view2**, **view3**, **view4**
- The blue text is a template description, which can be copied directly.

Sample of 3D Spatial Consistency



view1 view2 view3 view4

Question: As shown above

OptionA: (Red box, 1, 4, 3), (Yellow box, 3, 3, 2), (Green box, 5, 1, 2), (Blue box, 1, 4, 2), (Pink box, 4, 5, 1)

OptionB: (Red box, 5, 4, 2), (Yellow box, 3, 3, 2), (Green box, 1, 1, 3), (Blue box, 1, 4, 2), (Pink box, 4, 5, 1)

OptionC: (Red box, 1, 4, 3), (Yellow box, 1, 4, 2), (Green box, 4, 1, 2), (Blue box, 3, 3, 2), (Pink box, 5, 5, 2)

OptionD: (Red box, 1, 4, 3), (Yellow box, 1, 4, 2), (Green box, 5, 1, 2), (Blue box, 3, 3, 2), (Pink box, 4, 5, 1)

OptionE: (Red box, 1, 4, 3), (Yellow box, 1, 4, 2), (Green box, 4, 5, 2), (Blue box, 3, 3, 2), (Pink box, 5, 1, 2)

Figure 20: Example of *Spatial Cube Reasoning* from the BridgeV2 dataset. One reference view (here, **view1**) contains bounding boxes, and the model must infer the correct 3D coordinates of the objects across the synchronized views.

2052

2053

2054

2055

2056

2057

2058

2059

2060

2061

2062

2063

2064

2065

2066

2067

2068

2069

2070

2071

2072

2073

2074

2075

2076

2077

2078

2079

2080

2081

2082

2083

2084

2085

2086

2087

2088

2089

2090

2091

2092

2093

2094

2095

2096

2097

2098

2099

2100

2101

2102

2103

2104

2105



Template for Action Planning

Task: Which of the following operations is most likely to complete the task with the least collision? The following options are based on the **head** camera view. <Description of coordinate system definition>

Rules

- You can replace the **head** with **left-gripper** or **right-gripper**.
- The blue text is a template description, which can be copied directly.

Sample of Action Planning



left gripper view

head view

right gripper view

Question: If I want to pour water from the kettle on the table into the water cup. <Template which shown as above>

OptionA: Move the left gripper leftward, then forward, then downward to grasp the handle of the kettle. Then lift the kettle, move it upward, and then rightward to pour water into the cup.

OptionB: Move the left gripper rightward, then backward, then upward to grasp the handle of the kettle. Then lower the kettle, move it downward, and then leftward to pour water into the cup.

OptionC: Move the left gripper downward, then rightward, then forward to grasp the handle of the kettle. Then lift the kettle, move it forward, and then leftward to pour water into the cup.

OptionD: Move the left gripper forward, then leftward, then upward to grasp the handle of the kettle. Then lift the kettle, move it rightward, and then downward to pour water into the cup.

OptionE: Move the left gripper backward, then upward, then leftward to grasp the handle of the kettle. Then lift the kettle, move it downward, and then forward to pour water into the cup.

Figure 21: Example of *Planning* from the AgiWorld dataset. The model must select the correct sequence of normalized directional actions to accomplish the described task with minimal collisions.

2106

2107

2108

2109

2110

2111

2112

2113

2114

2115

2116

2117

2118

2119

2120

2121

2122

2123

2124

2125

2126

2127

2128

2129

2130

2131

2132

2133

2134

2135

2136

2137

2138

2139

2140

2141

2142

2143

2144

2145

2146

2147

2148

2149

2150

2151

2152

2153

2154

2155

2156

2157

2158

2159

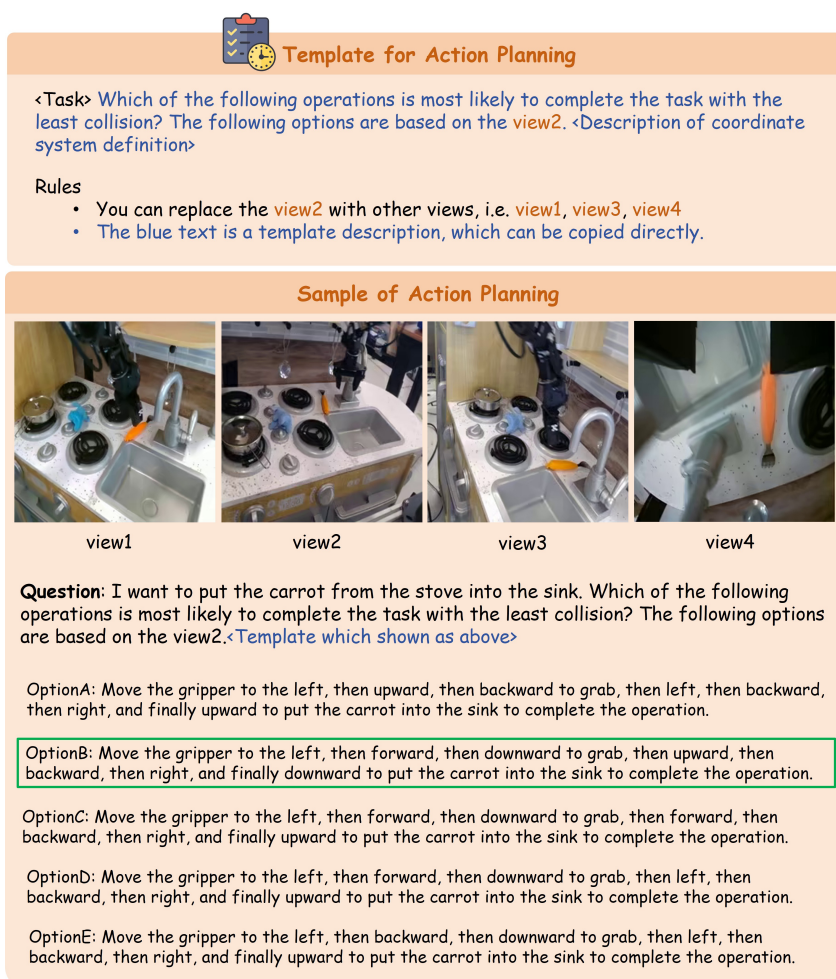


Figure 22: Example of *Planning* from the BridgeV2 dataset. One reference view (here, view2) is used to describe the options, and the model must infer the correct high-level sequence to achieve the task while avoiding collisions.

2160

2161

2162

2163

2164

2165

2166

2167

2168

2169

2170

2171

2172

2173

2174

2175

2176

2177

2178

2179

2180

2181

2182

2183

2184

2185

2186

2187

2188

2189

2190

2191

2192

2193

2194

2195

2196

2197

2198

2199

2200

2201

2202

2203

2204

2205

2206

2207

2208

2209

2210

2211

2212

2213


Template for Step Execution

<Task>, which of the following actions is most likely to accomplish this task? The following options are based on the **head** camera view. <Description of coordinate system definition>

Rules

- You can replace the **head** with **left-gripper** or **right gripper**.
- The blue text is a template description, which can be copied directly.

Sample for Step Execution



left gripper view



head view



right gripper view

Question: Suppose I want to use the right gripper to grab the spoon in the bowl. <Template which shown as above>

OptionA: Move the right gripper down and then to the left, then forward to grab.	OptionB: Move the right gripper up and then to the left, then forward to grab.	OptionC: Move the right gripper forward and then to the right, then down to grab.
OptionD: Move the right gripper down and then to the right, then forward to grab.	OptionE: Move the right gripper down and then to the left, then backward to grab.	

Figure 23: Example of *Execution* from the AgiWorld dataset. The model must select the correct primitive action, expressed in normalized directional terms, to complete the manipulation goal.

41

2214

2215

2216

2217

2218

2219

2220

2221

2222

2223

2224

2225

2226

2227

2228

2229

2230

2231

2232

2233

2234

2235

2236

2237

2238

2239

2240

2241

2242

2243

2244

2245

2246

2247

2248

2249

2250

2251

2252

2253

2254

2255

2256

2257

2258

2259

2260

2261

2262

2263

2264

2265

2266

2267

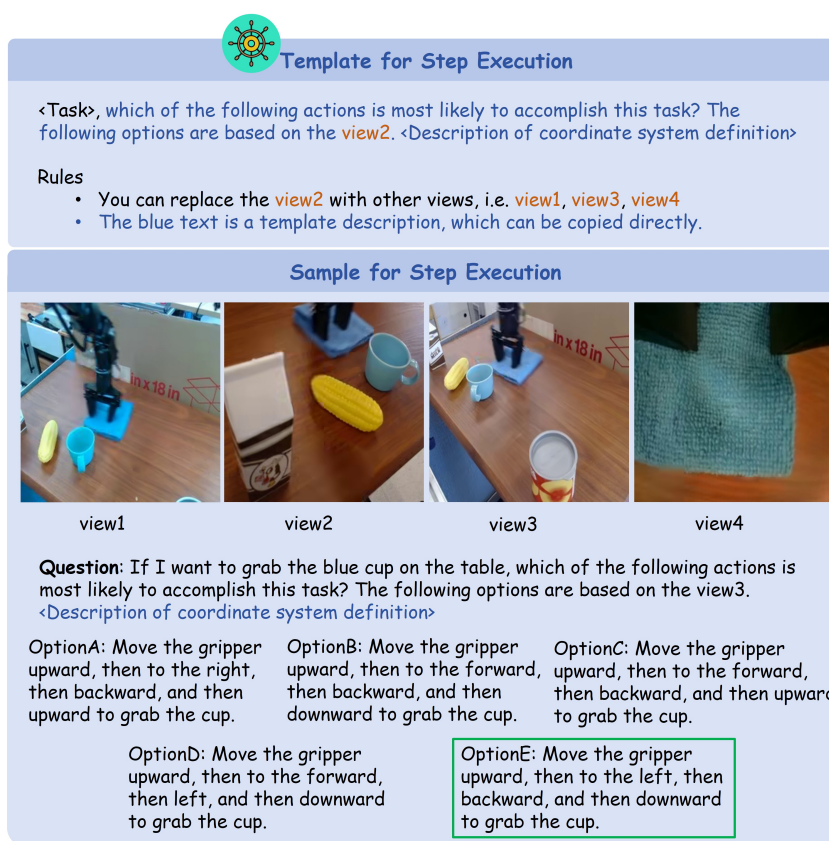


Figure 24: Example of *Execution* from the BridgeV2 dataset. One reference view (here, **view3**) is used to describe the options, and the model must identify the correct low-level action sequence to accomplish the given task.

2268
2269
2270
2271
2272
2273
2274
2275
2276
2277
2278
2279

2280

 **Template for Trajectory Selection**

2281 You are given three synchronized views—the left-gripper camera, the
2282 head camera, and the right-gripper camera. <Task>, which color track
2283 is most likely to complete the task?
2284

2285

2286 **Rules**

2287 • The blue text is a template description, which can be copied
2288 directly.

2289

2290

2291

2292

2293

2294

2295

2296

2297

2298

2299

2300

2301

2302

2303

2304

2305

2306

2307

2308

2309

2310

2311

2312

2313

2314

2315

2316

2317

2318

2319

2320

2321

2322

2323

2324

2325

2326

2327

2328

2329

2330

2331

2332

2333

2334

2335

2336

2337

2338

2339

2340

2341

2342

2343

2344

2345

2346

2347

2348

2349

2350

2351

2352

2353

2354

2355

2356

2357

2358

2359

2360

2361

2362

2363

2364

2365

2366

2367

2368

2369

2370

2371

2372

2373

2374

2375

2376

2377

2378

2379

2380

2381

2382

2383

2384

2385

2386

2387

2388

2389

2390

2391

2392

2393

2394

2395

2396

2397

2398

2399

2400

2401

2402

2403

2404

2405

2406

2407

2408

2409

2410

2411

2412

2413

2414

2415

2416

2417

2418

2419

2420

2421

2422

2423

2424

2425

2426

2427

2428

2429

2430

2431

2432

2433

2434

2435

2436

2437

2438

2439

2440

2441

2442

2443

2444

2445

2446

2447

2448

2449

2450

2451

2452

2453

2454

2455

2456

2457

2458

2459

2460

2461

2462

2463

2464

2465

2466

2467

2468

2469

2470

2471

2472

2473

2474

2475

2476

2477

2478

2479

2480

2481

2482

2483

2484

2485

2486

2487

2488

2489

2490

2491

2492

2493

2494

2495

2496

2497

2498

2499

2500

2501

2502

2503

2504

2505

2506

2507

2508

2509

2510

2511

2512

2513

2514

2515

2516

2517

2518

2519

2520

2521

2522

2523

2524

2525

2526

2527

2528

2529

2530

2531

2532

2533

2534

2535

2536

2537

2538

2539

2540

2541

2542

2543

2544

2545

2546

2547

2548

2549

2550

2551

2552

2553

2554

2555

2556

2557

2558

2559

2560

2561

2562

2563

2564

2565

2566

2567

2568

2569

2570

2571

2572

2573

2574

2575

2576

2577

2578

2579

2580

2581

2582

2583

2584

2585

2586

2587

2588

2589

2590

2591

2592

2593

2594

2595

2596

2597

2598

2599

2600

2601

2602

2603

2604

2605

2606

2607

2608

2609

2610

2611

2612

2613

2614

2615

2616

2617

2618

2619

2620

2621

2622

2623

2624

2625

2626

2627

2628

2629

2630

2631

2632

2633

2634

2635

2636

2637

2638

2639

2640

2641

2642

2643

2644

2645

2646

2647

2648

2649

2650

2651

2652

2653

2654

2655

2656

2657

2658

2659

2660

2661

2662

2663

2664

2665

2666

2667

2668

2669

2670

2671

2672

2673

2674

2675

2676

2677

2678

2679

2680

2681

2682

2683

2684

2685

2686

2687

2688

2689

2690

2691

2692

2693

2694

2695

2696

2697

2698

2699

2700

2701

2702

2703

2704

2705

2706

2707

2708

2709

2710

2711

2712

2713

2714

2715

2716

2717

2718

2719

2720

2721

2722

2723

2724

2725

2726

2727

2728

2729

2730

2731

2732

2733

2734

2735

2736

2737

2738

2739

2740

2741

2742

2743

2744

2745

2746

2747

2748

2749

2750

2751

2752

2753

2754

2755

2756

2757

2758

2759

2760

2761

2762

2763

2764

2765

2766

2767

2768

2769

2770

2771

2772

2773

2774

2775

2776

2777

2778

2779

2780

2781

2782

2783

2784

2785

2786

2787

2788

2789

2790

2791

2792

2793

2794

2795

2796

2797

2798

2799

2800

2801

2802

2803

2804

2805

2806

2807

2808

2809

2810

2811

2812

2813

2814

2815

2816

2817

2818

2819

2820

2821

2822

2823

2824

2825

2826

2827

2828

2829

2830

2831

2832

2833

2834

2835

2836

2837

2838

2839

2840

2841

2842

2843

2844

2845

2846

2847

2848

2849

2850

2851

2852

2853

2854

2855

2856

2857

2858

2859

2860

2861

2862

2863

2864

2865

2866

2867

2868

2869

2870

2871

2872

2873

2874

2875

2876

2877

2878

2879

2880

2881

2882

2883

2884

2885

2886

2887

2888

2889

2890

2891

2892

2893

2894

2895

2896

2897

2898

2899

2900

2901

2902

2903

2904

2905

2906

2907

2908

2909

2910

2911

2912

2913

2914

2915

2916

2917

2918

2919

2920

2921

2922

2923

2924

2925

2926

2927

2928

2929

2930

2931

2932

2933

2934

2935

2936

2937

2938

2939

2940

2941

2942

2943

2944

2945

2946

2947

2948

2949

2950

2951

2952

2953

2954

2955

2956

2957

2958

2959

2960

2961

2962

2963

2964

2965

2966

2967

2968

2969

2970

2971

2972

2973

2974

2975

2976

2977

2978

2979

2980

2981

2982

2983

2984

2985

2986

2987

2988

2989

2990

2991

2992

2993

2994

2995

2996

2997

2998

2999

3000

3001

3002

3003

3004

3005

3006

3007

3008

3009

3010

3011

3012

3013

3014

3015

3016

3017

3018

3019

3020

3021

3022

3023

3024

3025

3026

3027

3028

3029

3030

3031

3032

3033

3034

3035

3036

3037

3038

3039

3040

3041

3042

3043

3044

3045

3046

3047

3048

3049

3050

3051

3052

3053

3054

3055

3056

3057

3058

3059

3060

3061

3062

3063

3064

3065

3066

3067

3068

3069

3070

3071

3072

3073

3074

3075

3076

3077

3078

3079

3080

3081

3082

3083

3084

3085

3086

3087

3088

3089

3090

3091

3092

3093

3094

3095

3096

3097

3098

3099

3100

3101

3102

3103

3104

3105

3106

3107

3108

3109

3110

3111

3112

3113

3114

3115

3116

3117

3118

3119

3120

3121

3122

3123

3124

3125

3126

3127

3128

3129

3130

3131

3132

3133

3134

3135

3136

3137

3138

3139

3140

3141

3142

3143

3144

3145

3146

3147

3148

3149

3150

3151

3152

3153

3154

3155

3156

3157

3158

3159

3160

3161

3162

3163

3164

3165

3166

3167

3168

3169

3170

3171

3172

3173

3174

3175

3176

3177

3178

3179

3180

3181

3182

3183

3184

3185

3186

3187

3188

3189

3190

3191

3192

3193

3194

3195

3196

3197

3198

3199

3200

3201

3202

3203

3204

3205

3206

3207

3208

3209

3210

3211

3212

3213

3214

3215

3216

3217

3218

3219

3220

3221

3222

3223

3224

3225

3226

3227

3228

3229

3230

3231

3232

3233

3234

3235

3236

3237

3238

3239

3240

3241

3242

3243

3244

3245

3246

3247

3248

3249

3250

3251

3252

3253

3254

3255

3256

3257

3258

3259

3260

3261

3262

3263

3264

3265

3266

3267

3268

3269

3270

3271

3272

3273

3274

3275

3276

3277

3278

3279

3280

3281

3282

3283

3284

3285

3286

3287

3288

3289

3290

3291

3292

3293

3294

3295

3296

3297

3298

3299

3300

3301

3302

3303

3304

3305

3306

3307

3308

3309

3310

3311

3312

3313

3314

3315

3316

3317

3318

3319

3320

3321

3322

3323

3324

3325

3326

3327

3328

3329

3330

3331

3332

3333

3334

3335

3336

3337

3338

3339

3340

3341

3342

3343

3344

3345

3346

3347

3348

3349

3350

3351

3352

3353

3354

3355

3356

3357

3358

3359

3360

3361

3362

3363

3364

3365

3366

3367

3368

3369

3370

3371

3372

3373

3374

3375

3376

3377

3378

3379

3380

3381

3382

3383

3384

3385

3386

3387

3388

3389

3390

3391

3392

3393

3394

3395

3396

3397

3398

3399

3400

3401

3402

3403

3404

3405

3406

3407

3408

3409

3410

3411

3412

3413

3414

3415

3416

3417

3418

3419

3420

3421

3422

3423

3424

3425

3426

3427

3428

3429

3430

3431

3432

3433

3434

3435

3436

3437

3438

3439

3440

3441

3442

3443

3444

3445

3446

3447

3448

3449

3450

3451

3452

3453

3454

3455

3456

3457

3458

3459

3460

3461

3462

3463

3464

3465

3466

3467

3468

3469

3470

3471

3472

3473

3474

3475

3476

3477

3478

3479

3480

3481

3482

3483

3484

3485

3486

3487

3488

3489

3490

3491

3492

3493

3494

3495

3496

3497

3498

3499

3500

3501

3502

3503

3504

3505

3506

3507

3508

3509

3510

3511

3512

3513

3514

3515

<p

2322
 2323
 2324
 2325
 2326
 2327
 2328
 2329
 2330
 2331
 2332
 2333
 2334
 2335
 2336
 2337
 2338
 2339
 2340
 2341
 2342
 2343
 2344
 2345
 2346
 2347
 2348
 2349
 2350
 2351
 2352
 2353
 2354
 2355
 2356
 2357
 2358
 2359
 2360
 2361
 2362
 2363
 2364
 2365
 2366
 2367
 2368
 2369
 2370
 2371
 2372
 2373
 2374
 2375

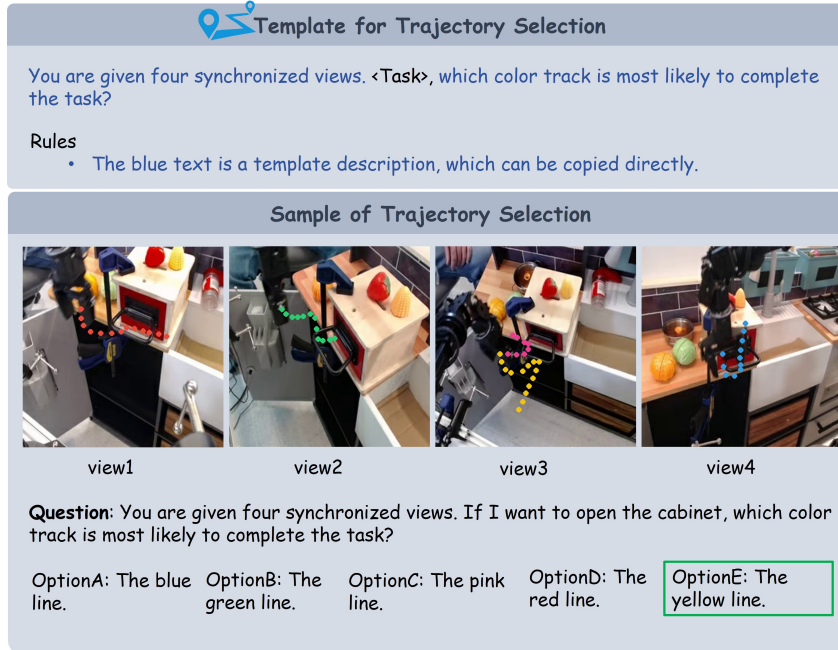


Figure 26: Example of *Trajectory Evaluation* from the BridgeV2 dataset. The model is given four synchronized views and must select the correct colored trajectory (here, the green line) that completes the described task.

2376

2377

2378

2379

2380

2381

2382

2383

2384

2385

2386

2387

2388

2389

2390

2391

2392

2393

2394

2395

2396

2397

2398

2399

2400

2401

2402

2403

2404

2405

2406

2407

2408

2409

2410

2411

2412

2413

2414

2415

2416

2417

2418

2419

2420

2421

2422

2423

2424

2425

2426

2427

2428

2429



Template for Affordance Recognition

You are given three synchronized views—the left-gripper camera, the head camera, and the right-gripper camera. Across these images, five grasp candidates are illustrated with color-coded lines—red, yellow, green, blue, and pink—such that each color appears exactly once, on one view only. The two endpoints of every line mark the intended positions of the gripper fingers. Which colour-coded line represents the grasp candidate most likely to succeed?

Rules

- The blue text is a template description, which can be copied directly.

Sample of Affordance Recognition



Question: As shown above

OptionA: Blue line.

OptionB: Green line.

OptionC: Pink line.

OptionD: Red line.

OptionE: Yellow line.

Figure 27: Example of *Affordance Recognition* from the AgiWorld dataset. Five color-coded grasp candidates are illustrated, and the model must select the one most likely to succeed.

2430
 2431
 2432
 2433
 2434
 2435
 2436
 2437
 2438
 2439
 2440
 2441
 2442
 2443
 2444
 2445
 2446

 **Template for Affordance Recognition**

You are given four synchronized views. Across these images, five grasp candidates are illustrated with color-coded lines—red, yellow, green, blue, and pink—such that each color appears exactly once, on one view only. The two endpoints of every line mark the intended positions of the gripper fingers. Which color-coded line represents the grasp candidate most likely to succeed?

Rules

- The blue text is a template description, which can be copied directly.

Sample of Affordance Recognition



view1 view2 view3 view4

Question: As shown above

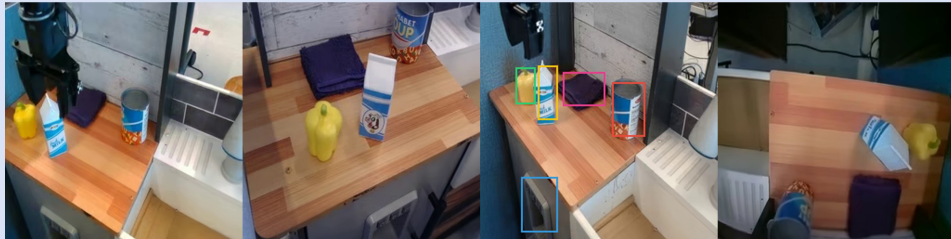
OptionA: Blue line.	OptionB: Green line.	OptionC: Pink line.
OptionD: Red line.	OptionE: Yellow line.	

2467 Figure 28: Example of *Affordance Recognition* from the BridgeV2 dataset. Grasp candidates are
 2468 distributed across four synchronized views, with the model required to select the most feasible op-
 2469 tion.

2470
 2471
 2472
 2473
 2474
 2475
 2476
 2477
 2478
 2479
 2480
 2481
 2482
 2483

2484
2485
2486
2487
2488
2489
2490
2491
2492
2493
2494
2495
2496
2497
2498
2499
2500
2501
2502
2503
2504
2505

Perceptual Hallucination / Grounding



"question": "You are given four synchronized views, only the view3 contains colored bounding boxes. Which option corresponds to the shortest grasping distance?

"A": "Grab the item in the red bounding box." (Model answer)

"D": "Grab the item in the yellow bounding box." (Correct)

Model response: To determine the shortest grasping distance, we need to consider the relative positions of the objects in the views. The view3 contains colored bounding boxes, which likely indicate the objects of interest for grasping.
1. **Red bounding box**: This box is around the yellow bottle.
2. **Pink bounding box**: This box is around the purple cloth.
3. **Green bounding box**: This box is around the blue bottle.
4. **Yellow bounding box**: This box is around the yellow bottle.
5. **Blue bounding box**: This box is around the blue bottle.
From the images, the yellow bottle is the same object in all views. The red bounding box in view3 is the closest to the yellow bottle in view4, indicating the shortest grasping distance.
Answer: A

Analyze: It mistook the red soup can for a "yellow bottle" and the green bell pepper for a "blue bottle." This is the most obvious "hallucination," directly proving that the small model failed at the Perception level.

2523
2524
2525
2526
2527
2528
2529
2530
2531
2532
2533
2534
2535
2536
2537

Figure 29: **Case Study 1: Perceptual Hallucination (Qwen2.5-VL-7B).** The model fails at basic visual grounding. As shown in the response, it explicitly misidentifies the red bounding box (a soup can) as a "yellow bottle" and the green box (a pepper) as a "blue bottle." This hallucination leads to a baseless conclusion, illustrating the perception bottleneck in smaller models.

2538
2539
2540
2541
2542
2543
2544
2545
2546
2547

Instance-level Correspondence



2548 "question": "In the right-gripper camera view, the item is outlined with a red bounding box.
2549 Which colored bounding box encloses that same item in the left-gripper camera view and
2550 the head camera view?"

2551 "B": "The yellow bounding box." (Model answer) "E": "The blue bounding box. (Correct)"

2553 Model response: To determine which colored bounding box encloses the same item in both
2554 the left-gripper camera view and the head camera view as the red bounding box in the
2555 right-gripper camera view, let's follow these steps:
2556 1. Identify the item within the red bounding box in the right-gripper camera view. It appears to be a yellow bell
2557 pepper.
2558 2. Locate the yellow bell pepper in the left-gripper camera view. It is enclosed
2559 by the pink bounding box.
2560 3. Confirm the location of the yellow bell pepper in the head
2561 camera view. It is enclosed by the yellow bounding box.
2562 Given this analysis, the item outlined by the red bounding box in the right-gripper camera view corresponds to the
2563 pink bounding box in the left-gripper camera view and the yellow bounding box in the
2564 head camera view.
2565 Since the question asks for the color of the bounding box that
2566 encloses the same item in both the left-gripper camera view and the head camera view,
2567 we need to identify the common item and its corresponding bounding box colors. The
2568 yellow bell pepper is consistently identified by the yellow bounding box in the head
2569 camera view.
2570 Therefore, the correct answer is:
2571 Answer: B

2572 Analyze: The main problem here is that the model first identifies what the object is
2573 when making its judgment. However, in this scene, there are many identical objects. The
2574 model must correctly identify the correct object based on spatial location and multi-view
2575 consistency. This turns it into a simple object recognition problem.

2576
2577
2578
2579
2580
2581
2582
2583
2584
2585
2586
2587
2588
2589
2590
2591

Figure 30: **Case Study 2: Instance-Level Correspondence Failure (Qwen2.5-VL-72B).** The scene contains multiple instances of the same class (yellow peppers). The model correctly identifies the category but fails to perform geometric alignment. It selects Option B solely because it contains a "yellow bell pepper," effectively reducing the multi-view consistency task to a simple object recognition problem.

2592

2593

2594

2595

2596

2597

2598

2599

2600

2601

2602

2603

2604

2605

2606

2607

2608

2609

2610

2611

2612

2613

2614

2615

2616

2617

2618

2619

2620

2621

2622

2623

2624

2625

2626

2627

2628

2629

2630

2631

2632

2633

2634

2635

2636

2637

2638

2639

2640

2641

2642

2643

2644

2645

Frame-of-reference / Single-view Bias



"question": "If I want to pour water into the cup, which of the following operations is most likely to complete the task with the least collision? The following options are based on the [left gripper camera view](#). <The definition of Coordinate>

"A": "Move the left gripper forward, then left, and then downward to grasp the handle of the kettle. Then move upward, and then forward to pour water into the cup.", (Model Answer)

"E": "Move the left gripper backward, then left, and then downward to grasp the handle of the kettle. Then move upward, and then forward to pour water into the cup." (Correct)

Model response: Step 1: Reasoning\n- Goal: Grasp the kettle handle with the left gripper and then pour into the cup with minimal collision.\n- From the head view, the kettle is on the left side with its handle on the far-left; the cup is near the center. From the left-gripper view, the right gripper/arm is ahead and slightly to the right, so moving right increases collision risk, while moving left avoids it.\n- Safe approach to the handle:\n- Move forward (+y) toward the kettle.\n- Then move left (-x) to align with the handle on the kettle's left side, steering away from the right arm.\n- Then move downward (-z) to grasp the handle near the table surface.\n- After grasping, lifting upward (+z) and moving forward (+y) toward the cup positions the kettle to pour.\n\nWhy others are less suitable:\n- B: Moving right heads toward the right gripper and tissue box; "upward to grasp" is incorrect since the handle is lower.\n- C: Downward then upward before grasping is unnecessary and risky near the table; lacks lateral alignment with the handle.\n- D: Moving right first increases collision risk with the right gripper; the right-then-left path is inefficient.\n- E: Moving backward moves away from the kettle, not toward it; adds unnecessary motion.\n\nStep 2: Best option\nAnswer: A

Analyze: GPT-5 interprets "moving forward" as reaching for the cup (based on the intuition of the Head View), but in the Left Gripper coordinate system, "moving forward" actually means passing over the cup, and going any further down would make it impossible to grab it. This perfectly explains "reference frame confusion" and "single-view offset".

Figure 31: **Case Study 3: Frame-of-Reference Error (GPT-5).** The task requires planning in the *Left-Gripper* frame. The model's reasoning ("Move forward ... toward the kettle") reveals a reliance on the global *Head View* intuition. In the specific local frame of the left gripper, "Forward" actually leads to a collision with the cup, while the correct action is to move "Backward" (Option E).